

January 2013

Kelvin Probe Electrode for Contactless Potential Measurement on Concrete-Properties and Applications

Michael Thomas Walsh

University of South Florida, mtwalsh@mail.usf.edu

Follow this and additional works at: <http://scholarcommons.usf.edu/etd>

 Part of the [Chemical Engineering Commons](#), [Civil Engineering Commons](#), and the [Materials Science and Engineering Commons](#)

Scholar Commons Citation

Walsh, Michael Thomas, "Kelvin Probe Electrode for Contactless Potential Measurement on Concrete-Properties and Applications" (2013). *Graduate Theses and Dissertations*.
<http://scholarcommons.usf.edu/etd/4850>

This Thesis is brought to you for free and open access by the Graduate School at Scholar Commons. It has been accepted for inclusion in Graduate Theses and Dissertations by an authorized administrator of Scholar Commons. For more information, please contact scholarcommons@usf.edu.

Kelvin Probe Electrode for Contactless Potential Measurement on Concrete –
Properties and Applications

by

Michael T. Walsh

A thesis submitted in partial fulfillment
of the requirements for the degree of
Master of Science in Civil Engineering
Department of Civil and Environmental Engineering
College of Engineering
University of South Florida

Major Professor: Alberto A. Sagiúes, Ph.D.
Babu Joseph, Ph.D.
Rajan Sen, Ph.D.

Date of Approval:
November 5, 2013

Keywords: Corrosion, Steel, Reinforcement, Polarization, Mapping

Copyright © 2013, Michael T. Walsh

DEDICATION

...to my wife, Jennifer and my son, Mickey.

ACKNOWLEDGMENTS

The guidance and assistance of Dr. A. A. Sagüés is greatly appreciated. The assistance with previous trial tests by Dr. Kingsley Lau is also appreciated.

A portion of the findings of this thesis constitute intellectual property related to a U.S. Utility Patent Application that was filed on May 30, 2013. Accordingly, the declaration “Patent Pending” must be associated with the device and technology associated with the embodiment described herein.

Some of the material contained in this thesis has been published in Corrosion Science, Vol 56, 2012, pp. 26-35 under the authorship of A.A. Sagüés and M.T. Walsh and appears in this document unchanged.

TABLE OF CONTENTS

| | |
|---|-----|
| LIST OF TABLES | iii |
| LIST OF FIGURES | iv |
| ABSTRACT..... | v |
| CHAPTER 1: INTRODUCTION | 1 |
| 1.1 Scope and Objectives | 1 |
| 1.2 Background | 2 |
| 1.3 Corrosion Basics | 3 |
| 1.3.1 Reaction Rates under Active Conditions | 4 |
| 1.3.2 Reaction Rates under Passive Conditions..... | 6 |
| 1.4 Concrete Surface Potential Measurement..... | 9 |
| 1.5 The Conventional “Wet-tip” Electrode..... | 12 |
| 1.6 The Kelvin Probe (KP) | 16 |
| 1.7 KP Comparison with Conventional “Wet-tip” Electrode | 21 |
| CHAPTER 2: METHODS | 24 |
| 2.1 Building a KP..... | 24 |
| 2.2 Making Test Specimens | 26 |
| 2.3 Measuring Potential | 29 |
| 2.4 Measuring Polarization Response..... | 31 |
| CHAPTER 3: RESULTS | 34 |
| 3.1 Potential Measurement Stability..... | 34 |
| 3.2 Effective Working Surface Position | 36 |
| 3.3 Working Distance Sensitivity | 39 |
| 3.4 Application: Potential Profile Mapping | 40 |
| 3.4.1 Short Term Repeatability..... | 42 |
| 3.4.2 Profile Correlation | 43 |
| 3.4.3 KP-Dry Profile Offset..... | 44 |
| 3.4.4 Spatial Variability of Observed Potential Values | 45 |
| 3.4.5 Concrete Moisture Condition..... | 46 |
| 3.5 Application: Polarization Response Measurement | 47 |
| 3.5.1 Baseline Potential Measurements | 47 |
| 3.5.2 Dynamic Polarization Measurements | 48 |
| CHAPTER 4: COMMENTS..... | 53 |

| | |
|--|----|
| CHAPTER 5: CONCLUSIONS | 57 |
| REFERENCES | 59 |
| APPENDICES | 62 |
| Appendix A Permission for Use of Table and Figures | 63 |
| Appendix B Permission for Use of Excerpts | 64 |

LIST OF TABLES

| | |
|--|----|
| Table 1 Concrete mixture proportions | 26 |
| Table 2 Baseline potential measurements | 48 |
| Table 3 Summary of dynamic polarization measurements | 52 |

LIST OF FIGURES

| | | |
|-----------|---|----|
| Figure 1 | Reaction rate i as functions of potential E | 5 |
| Figure 2 | Potential E as a function of reaction rate i | 6 |
| Figure 3 | Mixed potentials E_p and E_a | 8 |
| Figure 4 | Concrete surface potential measurement..... | 10 |
| Figure 5 | Potential map equipment configuration..... | 10 |
| Figure 6 | Potential map of concrete deck..... | 11 |
| Figure 7 | Section view of a conventional Cu-CuSO ₄ reference electrode with sponge | 12 |
| Figure 8 | Schematic diagram of half-cell potential measurement when using a CSE..... | 14 |
| Figure 9 | Schematic diagram of the Kelvin Probe as implemented in this investigation | 17 |
| Figure 10 | Schematic diagram of concrete surface potential measurement when using KP | 20 |
| Figure 11 | Test specimen dimensions and features | 27 |
| Figure 12 | Schematic diagram of enhanced KP plus dry counter electrode system..... | 32 |
| Figure 13 | Stability of measured potential for KP and SCE..... | 35 |
| Figure 14 | V_{OB}^{-1} as a function of h | 38 |
| Figure 15 | Change in potential as a function of working distance..... | 40 |
| Figure 16 | Potential profiles associated with steel in concrete beams A and B..... | 41 |
| Figure 17 | Linear correspondence between KP and SCE potential measurement values | 43 |
| Figure 18 | System response to galvanostatic pulses as measured by KP and SCE | 49 |
| Figure 19 | Analog circuit corresponding to corroding system | 50 |
| Figure 20 | Comparison between KP and SCE galvanostatic pulse polarization results..... | 52 |

ABSTRACT

The practical feasibility of using a Kelvin Probe as a novel reference electrode in the measurement of both potential and polarization pulse response of reinforcing steel in concrete is demonstrated. Potential values measured using a KP reflect greater stability and repeatability than can typically be attained with conventional reference electrodes. Duplicate reinforced concrete beam test specimens with well-differentiated centrally corroding rebar segments were analyzed using both the Kelvin Probe (KP) and a conventional Saturated Calomel Electrode (SCE). Potential profile maps were developed using potential values recorded under static conditions with both the SCE and the KP. Nominal polarization resistance was obtained using potential values recorded under dynamic polarization in both the active and passive regions using the KP and the SCE in conjunction with a customized counter electrode that applied a small galvanostatic polarizing current. In all cases the observed static potential values and dynamic potential response and recovery curves observed using the KP were consistent in shape and magnitude with those observed using conventional reference electrodes.

CHAPTER 1: INTRODUCTION

1.1 Scope and Objectives

The presence of various liquid junction potentials that emerge when a conventional reference electrode's electrolyte infiltrates the surface and bulk of a steel reinforced concrete structure causes the observed potential to drift. This drift prevents accurate potential measurement prior to system stabilization and it also precludes the attainment of an acceptable level of repeatability in cases where a long stabilization time is not permissible. This thesis shows not only that a Kelvin probe (KP) can be reliably used to measure the potential of reinforcing steel in concrete, but that its use eliminates the need for a stabilization period and accordingly provides a level of repeatability not typically attainable with a conventional reference electrode.

As a KP had not yet, to the author's knowledge, been used in an application of this type, fundamental operating parameters (e.g. working distance) had to be evaluated and established. In addition, inherent system functional characteristics (e.g. working surface depth) had to be verified and validated. Ultimately, the current work intended to demonstrate that:

- The KP can function as a reference electrode in the measurement of electrical potential of steel reinforcement embedded in concrete for both static potential measurements (e.g. as in potential profiling/mapping) and dynamic measurements (e.g. as in polarization pulse response when combined with a suitable counter electrode).
- The potential profiles and polarization response curves obtained using the KP in the evaluation of test specimens that were representative in material and geometry of typical

structures of interest are comparable in shape and range to those obtained using a conventional reference electrode.

- The KP can be used in cases that involve either dry or wet concrete surface conditions.
- The use of the KP can provide a nearly instantaneous indication of potential; the observed potential values will show a greater level of repeatability than that of values obtained using a conventional reference electrode on a similar time scale.
- The observed potential (i.e. that of the so-called working surface) is that of a plane that closely approaches the outer concrete surface regardless of concrete age and surface resistivity.
- The observed potential does not vary significantly with changes in the distance between the KP disk (i.e. the so-called reference surface) and the working surface.
- The KP behavior under the above conditions is consistent with expectations derived from theoretical analysis of the system.

1.2 Background

Corrosion and its associated remediation exert substantial influence on the economies of developed countries worldwide. According to a Federal Highway Administration (FHWA) corrosion cost study conducted in 2002, the estimated direct annual costs of corrosion in the United States exceeded \$275 billion, a figure that amounts to more than 3% of the nation's gross domestic product. The costs of corrosion in the industrial sectors such as utilities, transportation, infrastructure, production and manufacturing, and government account for approximately half of the total [1].

A significant part of the total cost of corrosion in the transportation and infrastructure categories is associated with the corrosion of steel reinforcing bars (rebars) placed to add strength to concrete that is used in the construction of bridges, dams, tunnels, etc. Active corrosion of steel effectively reduces the cross section of the rebars and eventually lowers the structure's load-carrying capacity. In addition, the expansive nature of the corrosion products causes concrete cover to spall even before significant rebar section loss occurs. Both of these deterioration modes reduce the structure's performance and longevity. Affected structures need maintenance, repair, and in some cases complete replacement. The FHWA study identified corrosion of steel reinforcement as the cause of structural deficiency in approximately 15% of highway bridges in the U.S. and determined the direct annual cost of corrosion in highway bridges to be \$8.3 billion. Notably, the indirect societal cost (associated with things like fuel and lost work time) was estimated to be as much as ten times this amount [1].

As corrosion involves electrochemical reactions, it can be detected by electrochemical means. Electrochemical corrosion analysis involves direct observation of the electrical current generated by a corroding system and can provide a convenient and effective means by which corrosion can be detected and evaluated even very early in its development. Detection equipment can not only identify and locate sites of active corrosion but can, in conjunction with an external current or voltage source, be used to estimate the actual rate of corrosion. Electrochemical methods are most easily understood in terms of the underlying phenomena of the corrosion process which are described below.

1.3 Corrosion Basics

A metal which has been separated from its natural compounds by smelting or some other means will tend over time to return to its natural condition [2]. While this process is one of

corrosion's main manifestations, corrosion can also be described the “attack (chemical) of a material by reaction with the environment with an associated deterioration of properties” [3].

All corroding systems have four components: 1. an electrolyte that enables movement of ions, 2. an anodic reaction that effectively dissolves the metal, 3. a cathodic reaction that consumes electrons generated by the anodic reaction, and 4. an electronic path by which electrons can move between the anodic and cathodic regions [2]. If corrosion occurs in the rebar of a reinforced concrete structure, the concrete pore solution provides the electrolyte and the rebar itself provides the path for electrons. Iron oxidation, the primary anodic reaction, advances according to



and oxygen reduction, the dominant cathodic reaction, follows



Corrosion can occur and proceed only while each and every one of these four components is present.

1.3.1 Reaction Rates under Active Conditions

Electrochemical reaction rates are expressed either in terms of mass lost per unit area per unit time (moles/cm²·s) or more commonly as metal loss in the form of an electrical current density (μA/cm²) described by a Faradaic conversion according to:

$$i = nF \cdot (\text{reaction rate}) \quad \text{Eq. 3}$$

where n = the valence of the affected metal, F = Faraday's Constant (~96,500 Coulomb/mole of electrons), and the reaction rate is equal to the quotient of the mass lost per unit area and time.

The reaction rate itself depends on the value of the potential, E of the steel with respect to the electrolyte. As illustrated conceptually in Figure 1 and equivalently in Figure 2, elevating E (i.e.

making it more positive) increases the anodic reaction rate (which is represented by the blue dotted line) as the ejection of positively charged iron ions into the electrolyte is facilitated. Likewise, decreasing E (i.e. making it more negative) increases the cathodic reaction rate (represented by the green solid line) as more electrons are available.

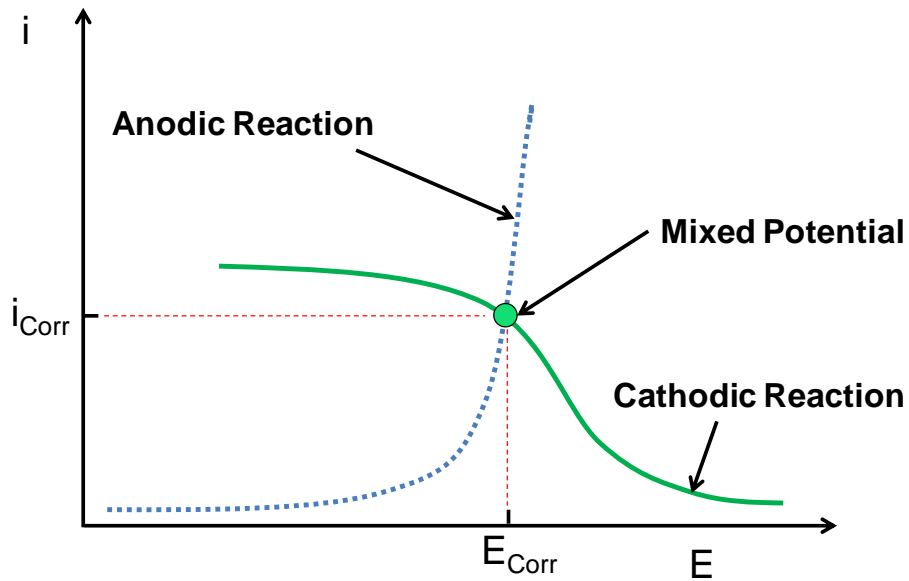


Figure 1 Reaction rate i as functions of potential E . Note that the anodic reaction rate (represented by the blue dotted line) increases as potential increases whereas the cathodic reaction rate (represented by the green solid line) increases as potential decreases. The intersection of the two lines indicates the “mixed potential” [2] described in the text.

In the absence of transport limitation of the available reacting species, a tendency of the anodic and cathodic reaction rates to increase and decrease exponentially with increasing potential was found by Tafel [4] [3]. It is therefore customary in corrosion engineering literature to represent the potential-current density relationship in the form of E - $\log i$ plots as shown in Figure 2. Accordingly, an exponential relationship appears as a straight line. If the reaction rate

is limited by reactant supply to the interface, as in the case of a cathodic reaction under partial transport control, the plot deviates somewhat from a straight line as illustrated in Figure 2 [4].

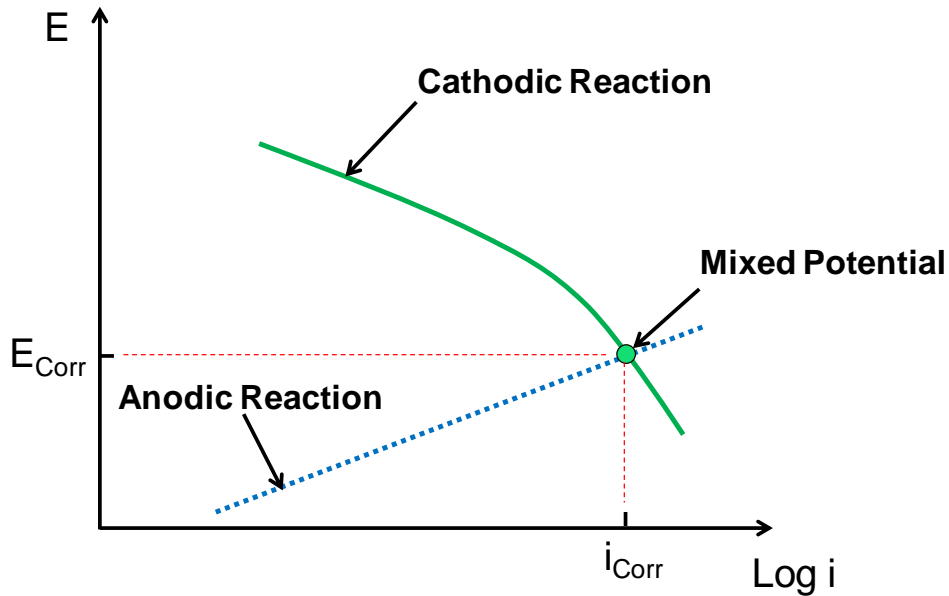


Figure 2 Potential E as a function of reaction rate i . Note that this figure presents the same information as Figure 1 rearranged to the format customary in corrosion engineering literature.

The intersection of the anodic and cathodic reaction lines in both Figure 1 and Figure 2 corresponds to the *mixed potential* or *corrosion potential* condition. At this point the rate at which electrons are produced by the anodic reaction exactly matches the rate at which they're consumed by cathodic reaction [2]. This is the steady state potential value assumed by a metallic component under freely corroding conditions.

1.3.2 Reaction Rates under Passive Conditions

While steel in direct contact with water can corrode spontaneously, steel embedded in concrete is normally protected from corrosion by a film that forms on its surface upon contact

with the alkaline ($\text{pH} > 12$) concrete pore water solution. This *passive film* modifies the behavior of the interface such that the steel's anodic reaction rate over a broad potential range increases little with increasing potential [2], in a way approximated by the vertical portion of the red solid line in Figure 3, where the anodic current density is ideally fixed at a constant value i_p . The protection provided by the passive film can be lost (*passivity breakdown*) if the film itself is compromised by interaction with chloride ions (present in seawater and deicing salts) in a concentration that exceeds a certain threshold and/or by interaction with concrete pore solution that has a pH value less than approximately 12. The latter condition sometimes results from the process of carbonation wherein pore water interacts with atmospheric carbon dioxide and forms calcium carbonate effectively and substantially lowering the concentration of the OH^- ions.

In the presence of a cathodic reaction (represented by the green solid line in Figure 3), steel in a passive condition reaches a steady state mixed potential E_p corresponding with point P. In regions subject to passivity breakdown, the anodic reaction rate reverts to the behavior (represented by the dotted blue line in Figure 3) illustrated in Figure 1 and Figure 2, and the corroding system reaches a more negative steady state mixed potential E_a corresponding to point A [5] [6].

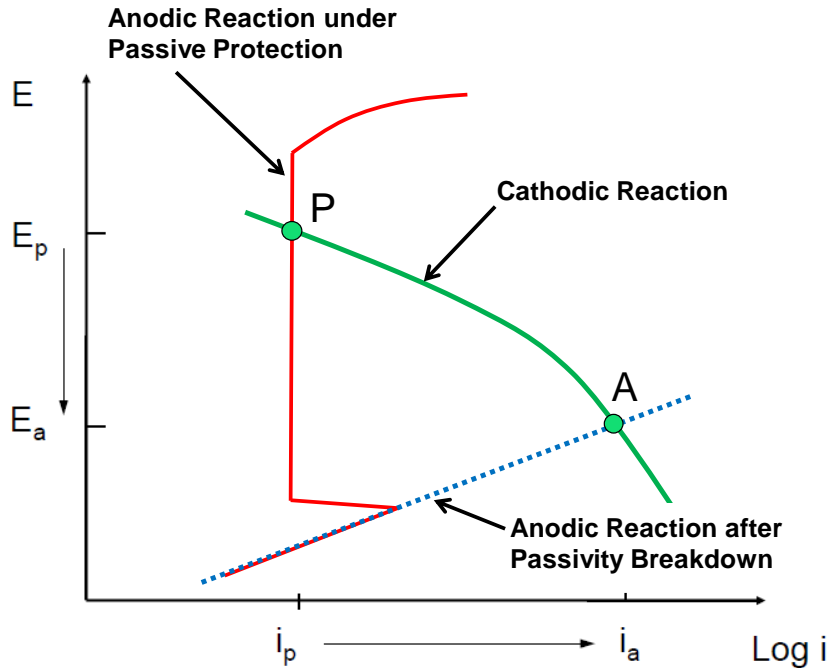


Figure 3 Mixed potentials E_p and E_a . The red solid line corresponds to the anodic reaction rate when the steel is protected by a passive film; the blue dotted line corresponds with the anodic reaction rate after passivity breakdown; the green solid line corresponds to the cathodic reaction rate in either case [2]. Point P represents the mixed potential of steel in the passive condition; point A represents the mixed potential of steel in the active condition.

The difference between the magnitudes of the two mixed potential values (E_p and E_a) illustrated in Figure 3 is the basis of a method [7] [8] [9] whereby the presence and location of actively corroding regions in a rebar assembly can be detected. As regions of the rebar assembly still in the passive condition will maintain elevated potentials near E_p while regions subject to passivity breakdown will develop more negative potentials near E_a , the value of the rebar potential with respect to the concrete can be used as an indication of the corrosion condition of the underlying steel. The potential values measured at the external concrete surface approximate those of the concrete adjacent to the rebar, thus permitting an external corrosion assessment as described below.

1.4 Concrete Surface Potential Measurement

Figure 4 schematically illustrates the method of concrete surface potential measurement mentioned above. As indicated in the figure, this method involves the use of a reference electrode and a voltmeter. The voltmeter must have a high input impedance to prevent any electrical current load introduced by the instrument from disturbing the potential of either the reference electrode or the steel-to-concrete interface. The combined polarization pattern whereby the localized region of active corrosion passivity breakdown is electrochemically coupled to the remaining passive steel surface is an example of a corrosion *macrocell*. The steady state potentials and corrosion current associated with such a configuration are referred to as the *macrocell potentials* and *macrocell current* respectively. Note that positive ions enter the concrete in the region of the corroding steel as the iron dissolves and that this gives rise to an electrolytic macrocell current which terminates with an associated ohmic potential difference at the concrete in the passive steel region. Given the customary [8] voltmeter polarity indicated in Figure 4, the potential observed at the concrete surface near steel covered by a passive film is less negative than that observed near steel that has undergone passivity breakdown.

The ASTM International *Standard Test Method for Corrosion Potential of Uncoated Reinforcing Steel in Concrete* (ASTM C876-09) [8] presents a procedure that is commonly used to systematically measure surface potential of reinforced concrete structural members. As indicated in the standard, localized corrosion typically manifests considerable change in potential (“hundreds of millivolts”) over relatively short distances (“a few hundred millimeters”). The standard, based on conditions prevalent on bridge decks subject to reinforcement corrosion, indicates that the probability of active corrosion is greater than 90% if observed potentials are more negative than -0.35 V CSE (i.e. Copper/Copper Sulfate Electrode; see Section 1.5), that the

probability of no corrosion is greater than 90% if potentials are more positive than -0.20 V CSE, and that corrosion activity cannot be characterized if the observed potential lies in the range between -0.20 and -0.35 V CSE. A schematic illustration of the equipment set-up prescribed by the Standard is presented in Figure 5.

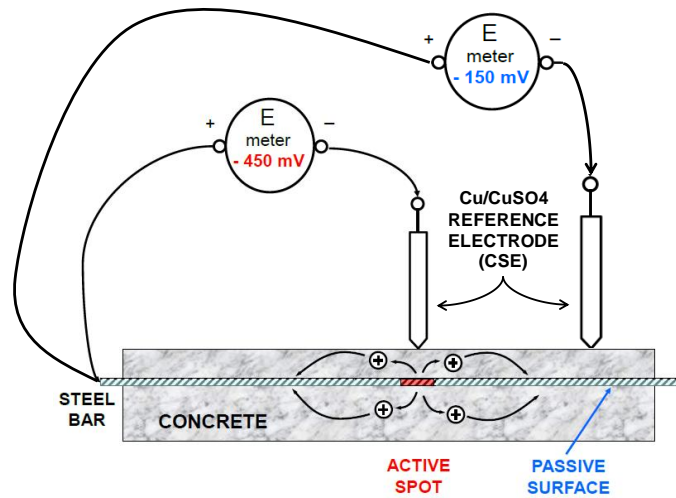


Figure 4 Concrete surface potential measurement [2]. Note the difference in magnitude of potential measurements made at different locations on the concrete surface. Steel in the “active spot” has undergone passivity breakdown and forms a corrosion macrocell with steel that has maintained its “passive surface”.

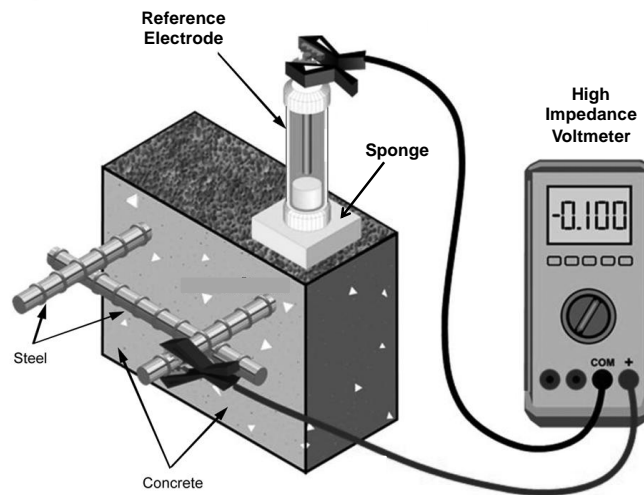


Figure 5 Potential map equipment configuration. (Schematic representation of half-cell potential measurement equipment arrangement from Fig. 1 of ASTM C876-09 [8].)

The test method, which involves measuring potential on the concrete surface at individual points of a grid-like array that encompasses the region of interest, is commonly applied to structures that use two dimensional arrays of interconnected rebar. The discrete potential values can be averaged and presented graphically in the form of a *potential map* to reflect the shape and distribution of corroding regions as indicated in Figure 6.

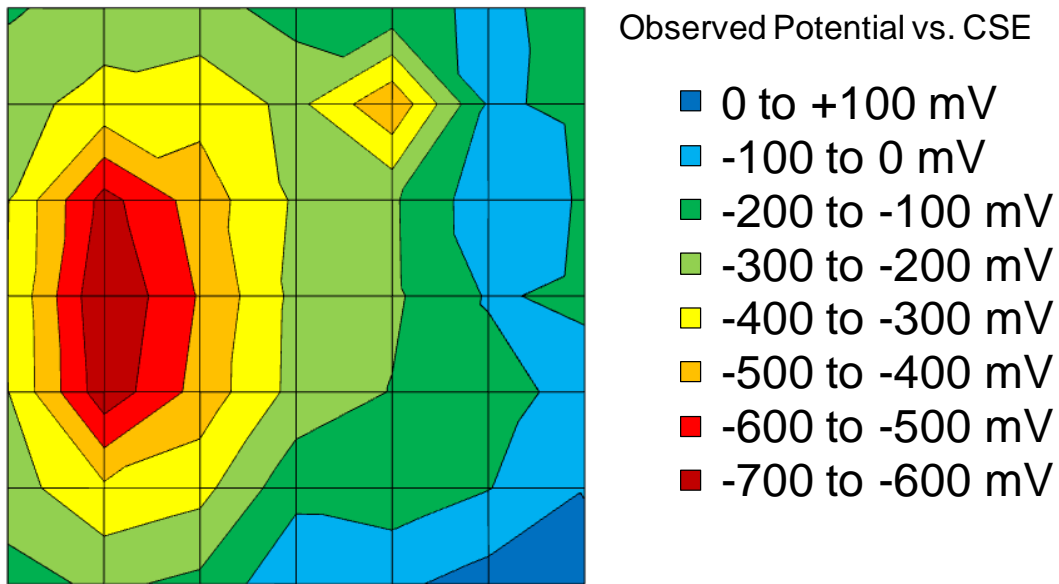


Figure 6 Potential map of concrete deck. Different colors correspond with different observed surface potentials. The steel in the region of the deck corresponding to the dark red area was known to be experiencing anodic reactions equivalent to active corrosion. The subject concrete deck consisted of an 8x8 ft, 5.5 inch thick concrete slab (clear cover depth: 2.5 inches) with a single mat of interconnected plain steel #4 rebar aligned parallel with the vertical edge of the figure on 6 inch centers. This map was made via MS Excel's Contour Chart application on 12-03-2011 using data obtained using a Copper-Copper Sulfate reference electrode (CSE).

In addition to their use in potential mapping, surface potential measurements form the basis of several other routine electrochemical corrosion analysis methods associated with the monitoring of cathodic protection systems, assessment of the effectiveness of corrosion repair patches, and determination of corrosion rate.

1.5 The Conventional “Wet-tip” Electrode

The use of a conventional “wet-tip” electrode introduces certain complications (discussed below) that served as the stimuli for exploring the use of the Kelvin Probe (KP) as an alternative reference electrode in this application. As the principle of operation and actual use of the KP itself are most easily understood after consideration of the electrochemical aspects of the measurement process and some specific interactions between the reference electrode and the corroding system, these issues are presently described in terms of a conventional electrode.

Figure 7 presents an illustration of a Copper-Copper Sulfate reference electrode (CSE), a conventional “wet-tip” electrode typical of the kind prescribed by ASTM C876 [8] for use in concrete surface potential mapping. The standard also prescribes the use of an *electrical junction device* which in most embodiments is a sponge soaked with an electrically conductive liquid. The combination of the electrolyte-saturated porous plug and the electrical junction device/sponge is a form of what is commonly referred to as a *salt bridge*.

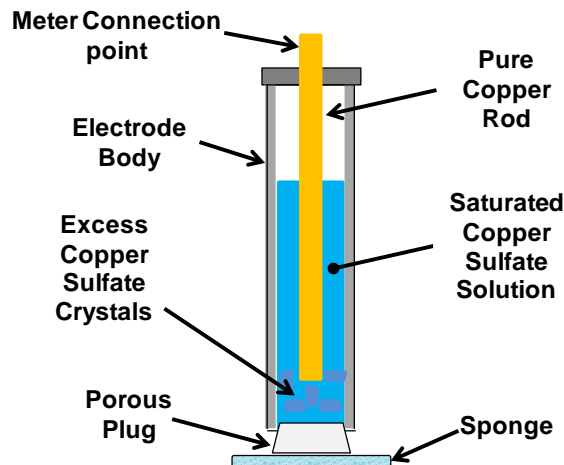


Figure 7 Section view of a conventional Cu-CuSO₄ reference electrode with sponge. Note that the sponge is moistened with a conductive liquid and that the electrode body is made of an insulating material.

The potential measurement process involves interfaces and interactions that necessitate consideration of various phenomena. First, it is noted that even under equilibrium conditions appreciable *interfacial potential* differences may develop when any two dissimilar materials (metals or electrolytes) come into contact. In the case of metal-to-metal contact, the potential difference arises as a consequence of the electron exchange associated with the equalization of the metals' different Fermi levels [10]. For metal-to-electrolyte interfaces, the potential difference is associated with specific electrochemical reactions between the metal and electrolyte such as the corrosion reactions discussed above. In the case of electrolyte-to-electrolyte interfaces, potential differences (called in this case *junction potentials*) arise given differences in both the diffusivity and concentration of ions in the electrolyte on each side of the interface.

The measurement of half-cell potential of steel in concrete using a “wet-tip” electrode involves several material interfaces and accordingly, several interfacial potentials. The interfaces between the measurement equipment and the steel/concrete system which were illustrated schematically in Figure 5 are represented with their associated interfacial potentials in Figure 8. It is noted that although copper wiring is used in the example in the figure, the overall conclusions are applicable in cases that use other materials or more complex arrangements.

A Galvani potential i.e. the amount of work per unit charge that would be required to transport a charged particle from a reference position located at an infinite distance in a vacuum to a point in the interior of the phase far¹ from the phase boundary, is associated with each phase illustrated in Figure 8. Each Galvani potential is identified in Figure 8 by the Greek letter Φ with an appropriate subscript. Four interfacial potential differences are also identified, each

¹ It is assumed that the phase is thick enough such that an interior bulk region can be delineated from a surface double-layer region. It is noted that Galvani potentials cannot be measured directly [10] but serve as point of reference for the measurable (Volta) potential. See section 1.6.

denoted by an X with a subscript. The arrows in the figure indicate polarity such that the interfacial potential difference is the difference between the Galvani potential at the head of the arrow and the Galvani potential at the tail.

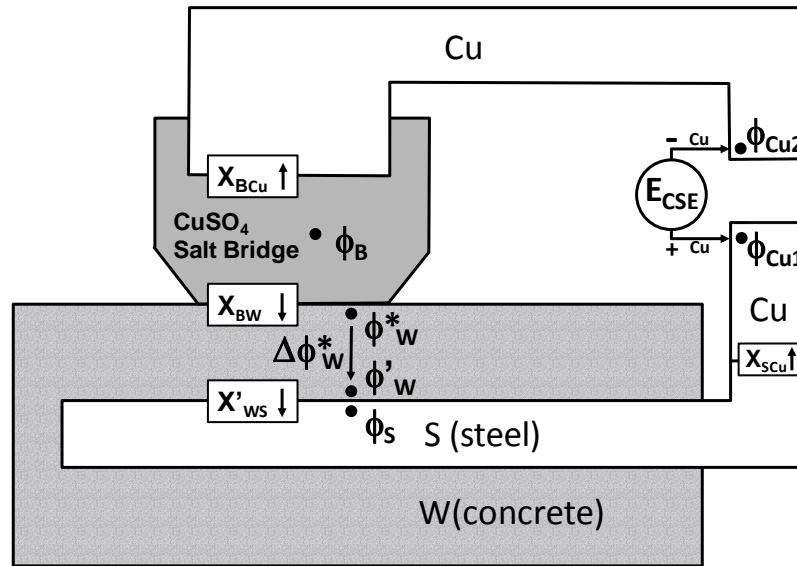


Figure 8 Schematic diagram of half-cell potential measurement when using a CSE. Note that W represents the water in the pore solution in the concrete, S represents the steel, and B represents the bulk of the electrolyte [25].

The potential, E_{CSE} indicated by the voltmeter is given by

$$E_{CSE} = \Phi_{Cu1} - \Phi_{Cu2} = X'_{WS} + X_{SCu} - X_{BCu} + X_{BW} + \Delta\Phi_w^* \quad \text{Eq. 4}$$

where X'_{WS} is the interfacial potential difference between the steel bar and the water in the concrete pores, X_{SCu} is the potential difference between the copper voltmeter lead and the steel bar, X_{BCu} is the potential difference between the bulk of the electrolyte in the salt bridge and the electrode (corresponding to the pure copper rod in

Figure 7), X_{BW} is the potential difference between the bulk of the electrolyte and the water in the pores, and $\Delta\Phi_w^*$ is the difference between Φ_w^* and Φ'_w which are in general not equal because of the ohmic potential difference created by the corrosion macrocell currents in the concrete and also because of electrolyte composition gradients within the concrete that cause macroscopic junction potentials and electrokinetic effects [11] [12]. Both Φ_w^* and Φ'_w are regarded as effective values, those of ideal conductors that would yield the same experimental results as those obtained in the concrete if the concrete was homogeneous. Accordingly, Φ_w^* and Φ'_w may be viewed as representing spatially averaged potential values in the localized regions of interest. Ohmic potential differences and similar effects within the metals themselves are treated as negligible in the present analysis.

The salt bridge lies between the bulk of the electrode's CuSO_4 solution and the surface of the concrete. The potential difference X_{BW} incorporates any diffusion potentials or related phenomena associated with ionic concentration gradients across the plug and sponge. The polarity chosen to designate X_{BCu} , a metal-electrolyte interfacial potential difference, was chosen to match that of X'_{wS} so both variables adhere to the usual electrochemical convention² [25].

It should be noted that the penetration of moisture and ionic species in the region of the concrete contacted by the wet sponge is not instantaneous and thus X_{BW} and $\Delta\Phi_w^*$ are regarded as time-dependent. This time dependence appears as measurement drift from the value observed when the sponge initially contacts the concrete surface.

² The usual electrochemical convention involves reporting the potential as the difference between the potentials of the metal and the electrolyte (i.e. $E \equiv E_M - E_E$) accounting also for an intervening electrode as appropriate [10].

As the moisture penetrates the concrete, the observed potential will be directly affected by the consequences of prior concrete surface alterations due to concrete carbonation, sulfate attack, weathering, and other environmental interactions. The extent and nature of measurement artifacts associated with these phenomena will be further obscured as the shared electrolyte link between the electrode's metallic terminal and the concrete pore water is subject to interdiffusion (if concrete pores are saturated) or strong convective capillary action (if pores are partially dry).

1.6 The Kelvin Probe (KP)

The KP is a device that determines the potential difference E between two surfaces designated as the working surface and the reference surface. Though the KP principle of operation has been described extensively in the literature [13] [14] [15] [16], some fundamental concepts are included here for clarity.

The working surface and the reference surface of a KP approximate the two plates of a parallel plate capacitor. In this application, the working surface is a small area on the outer concrete surface and the reference surface is the bottom side of a stainless steel disk (of e.g., 1 cm diameter) that faces the concrete surface and is positioned at a small distance h above it (see Figure 9).

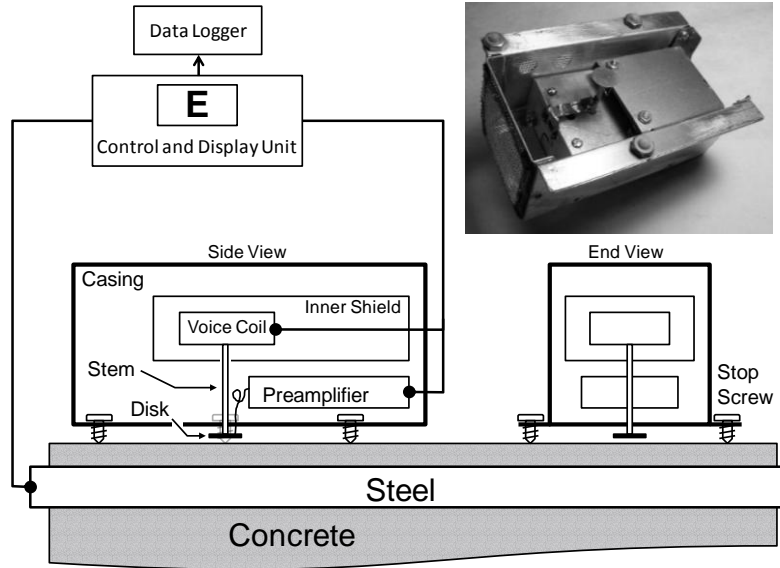


Figure 9 Schematic diagram of the Kelvin Probe as implemented in this investigation [25]. Note: Patent Pending.

The relationship between electrical charge Q and the potential difference E across a capacitor with capacitance C is described by the expression

$$Q = E C \quad \text{Eq. 5}$$

where C , for plates with a small gap, is approximated according to

$$C = \varepsilon \varepsilon_0 A/h \quad \text{Eq. 6}$$

where ε is the dielectric constant of the medium in the gap between the plates (for atmospheric air, $\varepsilon \approx 1$), ε_0 is the permittivity of vacuum, A is the one-sided surface area of the smallest of the plates (in this case the reference surface), and h is the distance between the plates.

In the current case, the value of E is fixed by characteristics of the components and interfaces in the electrical path between the working and reference surfaces. Any change in the height h of the disk (reference surface) above the concrete (working surface) will therefore necessitate a corresponding change in the value of Q in order to satisfy both equations (1) and (2). A cyclical variation of h would likewise cause a cyclical variation in Q and a cyclical

variation of Q would result in the circulation of an alternating current I_A through the conductive path³.

As illustrated in Figure 9, the disk is electronically connected to the steel bar embedded in the concrete. The surface of the steel bar is electrolytically connected, mainly via the water in the concrete pore network, with the external surface of the concrete. The concrete and the reference surfaces are thus joined through an electronic and electrolytic conductive path with associated interfaces that determine the value of E [25].

If a potential source with known potential E' is connected in series between the KP and the steel bar, the potential between the reference and concrete surface becomes $E+E'$. If $E'=-E$ the potential across the capacitor and the alternating current in the circuit both disappear [25]. The value of E can thus be directly indicated by varying E' and recording its value when the observed current $I_A=0$. The KP control and display component illustrated in Figure 9 provides the potential E' , electronic amplification for the observed signal, and a means by which E' can be varied and recorded either manually or automatically.

The interfaces between the KP equipment and the steel/concrete system which were illustrated schematically in Figure 9 are represented with their associated interfacial potentials in Figure 10. As was the case with the wet-tip electrode, the path of the potential measurement circuit has several interfacial potentials. It is important to note however that though the concrete and reference surfaces are joined by an electronic and electrolytic path as indicated above, the disk and concrete surface do not otherwise directly contact one another.

³In a dynamic condition E is not exactly constant due to interfacial polarization and ohmic drops caused by I_A , but its small value makes those effects correspondingly small. Regardless, they disappear at the zeroing condition as described in the text.

The concrete and reference surfaces interact via an electric field that arises between the two facing surfaces. This interaction necessitates consideration, for each surface, of the Volta (i.e. “outer” [13] [10]) potential i.e. the amount of work per unit charge that would be required to transport a charged particle from a reference position located at an infinite distance in a vacuum to a point just at the exterior of the phase, but not so close that image charges would become a source of uncertainty [10].

In the present case, the working and reference surfaces each have a Volta potential identified by the Greek letter ψ and an appropriate subscript. Proper consideration of Volta potentials requires that each interface has a well-defined boundary and a locally uniform electric charge profile. These conditions are adequately met by the metallic reference disk and it accordingly may be considered to have a well-defined spatially averaged ψ_R value. The concrete surface is however quite heterogeneous, as is the distribution in the concrete pore network of the electrolyte which is responsible for much of the electric charge configuration in the material. Hence ψ_W should be considered only as an effective value, that of an ideal conductor that would yield the same experimental results as those actually obtained and accordingly ψ_W may be viewed as representing an approximate average of the potential of the surface of the concrete beneath the footprint of the reference surface disk. Lateral heterogeneity up to the mm scale (pore space-paste-fine aggregate domain) is expected to be reasonably averaged beneath the disk, but some sensitivity to the distribution of the coarse-aggregate, with mean diameter greater than one centimeter, can be anticipated.

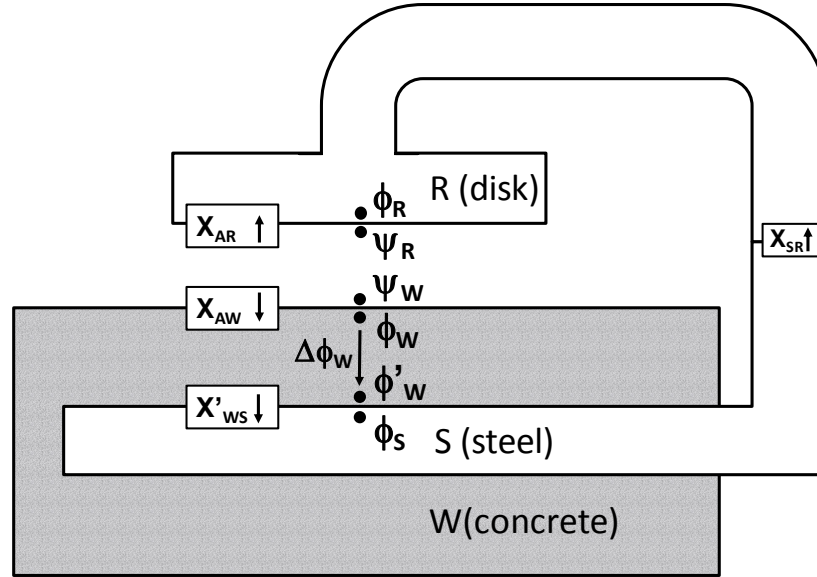


Figure 10 Schematic diagram of concrete surface potential measurement when using KP [25].

The potential E measured by the KP is the difference between the Volta potential ψ_R of the reference surface and the Volta potential ψ_W of the working surface, that is

$$E = \psi_R - \psi_W \quad \text{Eq. 7}$$

For simplicity, only two different metals are assumed to be involved, one for the reference surface (R) and one for the steel bar (S). The respective inner (Galvani [10]) potentials are designated Φ_R and Φ_S and the corresponding interfacial potential difference between them is described by $X_{SR} = \Phi_R - \Phi_S$. As in Figure 8, each difference of potential indicated in Figure 9 is added to the potential at the tail of the arrow to obtain the potential at the head of the arrow. The medium-to-air interfacial potential differences for the reference and concrete surfaces are $X_{AR} = \Phi_R - \psi_R$ and $X_{AW} = \Phi_W - \psi_W$ respectively and the metal-to-electrolyte

interfacial potential is $X'_{WS} = \Phi_S - \Phi'_W$. The value of $\Delta\Phi^*_W$ is the difference between Φ^*_W and Φ'_W which are in general not equal as described above.

Applying the above definitions to Eq. 7 yields

$$E = X'_{WS} + X_{SR} - X_{AR} + X_{AW} + \Delta\Phi_W \quad \text{Eq. 8 [25]}$$

1.7 KP Comparison with Conventional “Wet-tip” Electrode

Effective use of a wet-tip electrode necessitates an electrolytic interface between the electrode and the steel/concrete system. The establishment of this interface is inherently disruptive to the system as it involves infiltration of both liquid (e.g. water, electrolyte from the electrode, pre-wetting solution) and ions contained in the liquid. While this infiltration is unlikely to cause any significant change to X'_{WS} as long as the concrete cover depth exceeds a minimum value and the level of surface wetting is kept below a maximum value, the Galvani potential associated with the water in the undisturbed pore network, described by Φ_W in Figure 9, can be altered to a new value Φ^*_W as indicated in Figure 8. Given its contactless character, placement of the KP on the system should of course cause no significant deviation of X'_{WS} and $\Delta\Phi_W$ from their respective native values.

The potential measured by the KP can be related to potential measured in the usual manner with a CSE reference electrode by regarding X'_{WS} as invariant and evaluating Eqs. 4 and 8. This relationship is described by

$$E = E_{CSE} + [(X_{SR} - X_{SCu}) + (X_{AW} - X_{AR}) + X_{BCu} + \Delta\Phi_W] + [-X_{BW} - \Delta\Phi^*_W] \quad \text{Eq. 9 [25]}$$

The terms contained by the first set of square brackets are functions of the properties of metal-to-metal, metal-to-air and metal-to-solution interfaces, and of the condition of the concrete in the undisturbed condition. On first approximation and in a particular location on the concrete surface, these terms were regarded as constants of the system and their sum could constitute a simple constant addition term in conversions between E and E_{CSE} .

In contrast, the terms contained by the second set of square brackets vary as moisture and ionic species penetrate the concrete in the region affected by pre-wetting and subsequent contact by the wet-tip electrode and sponge. These terms were regarded as time dependent and their presence effectively precludes relating E and E_{CSE} through a simple time-invariant addition term.

While the variation should become inconsequential after moisture and ionic species distributions reach their respective steady states, these processes might involve substantial time periods [17]. As an alternative to waiting for steady state conditions, the system can be routinely examined after a prearranged time after surface wetting, when the time dependent terms have evolved to roughly reproducible values. This approach was adopted in the experiments presented here.

The above analysis can be extended to cases that also involve either pre-wetting the concrete surface prior to using the KP or the use of reference electrodes other than the CSE. If the concrete surface has been wetted prior to making potential measurements with a KP, both X_{AW} and $\Delta\Phi_W$ become time-dependent. As the value of $\Delta\Phi_W$ can be expected to be similar to $\Delta\Phi_W^*$, the influence of their combination on the value of E as described by Eq. (8) might be minimized. It should be noted however that pre-wetting the concrete surface can also affect X_{AR} as water could be adsorbed by the disk following transfer from the freshly wetted concrete

surface⁴ by evaporation. While it is true that the influence of the time dependent factors can be minimized by maintaining diligent and consistent control over the amount of pre-wetting and the time allowed to pass between pre-wetting and measurement, these circumstances underscore the complexities of the system that can significantly compromise repeatability.

It is noted that in addition to the issues mentioned above, a CSE might not be suitable in applications (e.g. statues, special architectural features) that cannot tolerate the blue copper sulfate solution residue stains that are often associated with its use.

The above analysis could apply to conventional electrodes other than the CSE (e.g. the Saturated Calomel Electrode (SCE) which uses the reaction between mercury and mercury (I) chloride in a saturated solution of potassium chloride in water [3]). The general above discussion applies equally in such cases but appropriate substitutions for X_{SCu} and X_{BCu} should be made as well as consideration for introduction of any other relevant metal-to-metal contact.

⁴ In lieu of more sophisticated treatment that would need to address the creation of other interfaces due to formation of a film or deposit, the combined effects are bundled for simplicity as an equivalent change in the effective value of X_{AR} . The same approach applies here to any electrode that has a passive film or any other compositional differences near the surface [25].

CHAPTER 2: METHODS

2.1 Building a KP

As indicated above, the fundamental operating principle of the KP involves bringing a reference surface into close proximity with a working surface and then causing it to oscillate between points of minimum and maximum distance from the working surface. Charge accumulates on both the reference and working surfaces when held in close proximity and this charge varies and induces an alternating current in the circuit when the reference disk oscillates.

KPs are used in several areas of modern technology [13] and can be purchased in several off-the-shelf configurations. The sizes and operating parameters of most commercially available KPs however differ from those required by the conditions associated with potential measurement on a concrete surface. These factors combined with high commercial unit acquisition cost prompted in-house fabrication of a suitable KP. Accordingly, a KP was designed and built in the lab using readily available materials and technology [13].

Fundamentally, a KP consists of four main components: a reference surface, a means to cause oscillation of the reference surface, a means by which the spatial relationship between the oscillating reference surface and the working surface can be established and maintained, and an electromagnetic shield. The reference surface was provided by a 13 mm diameter stainless steel (Type AISI 302) disk. The surface intended to face the working surface was polished to an 800-grit finish and was gently cleaned periodically with a cotton-tipped applicator dipped in ethyl alcohol. Oscillation capability was provided by a voice coil electromagnetic driver in the form

of a common audio speaker. The driver oscillated with amplitude $h_A = 0.5 \text{ mm} \pm 0.1 \text{ mm}$ (i.e. $1 \pm 0.2 \text{ mm}$ peak-to-peak), and frequency of 147 Hz in an approximately sinusoidal waveform. At rest, the distance between the reference and working surfaces (known as the “working distance”) was $h = 1 \text{ mm}$ yielding a nominal reference-to-working surface distance $h_C = h - h_A$ of approximately 0.5 mm. The disk was connected to the driver via a post made of wood which was selected for its ability to electrically isolate the disk from the driver while simultaneously being able to dissipate any static charge that might accumulate.

The assembly consisting of the driver, post, and disk was rigidly connected to a small aluminum box. The box served to contain all of the component parts while also providing a shield that protected the circuitry and internal parts from electromagnetic and environmental interference. The box featured three polymer adjustment screws on the side that faced the working surface. The screws, which were arranged in the shape of a triangle to provide stability, protruded from the bottom edge of the box such that an adjustable unshielded gap of approximately 4 mm was left between the box and the concrete surface. The screws enabled fine tuning of h to values within 0.1 mm of the desired value by gauging against a flat machined surface.

The nature of the nominally flat and smooth concrete surfaces associated with the experiments typically introduced $< 0.1 \text{ mm}$ additional uncertainty in the value of h . The sensing circuit detected the off-zero current with a circuit that approached a zero-resistance-ammeter configuration [13]. The rest of the electronic processing unit was a variation of that used by Klein [13]. The automatic zeroing function was provided by a feedback circuit, and the value of E was acquired digitally. The probe output was electronically filtered with a low pass filter with time constant $\tau \sim 1 \text{ s}$ [25].

2.2 Making Test Specimens

A test plan was developed to establish a means by which the KP's ability to measure the half-cell/open circuit potential of reinforcing steel in concrete could be evaluated. As the use of actual in-service or decommissioned reinforced concrete structures as test subjects would necessarily have involved uncertainties with regard to concrete constituent components, mixture proportions, mixing methods, materials, construction methods, and particular aspects of the operating environment (e.g. temperature, humidity, chemical exposure), dedicated test specimens were designed and constructed.

The test specimens consisted of two identical reinforced concrete beams of 70 cm length, 15 cm width, and 5 cm thickness. The concrete mix recipe is presented in Table 1. Each beam was reinforced by a single #4 plain steel ASTM A-615 bar with dark mill scale that was aligned with the lengthwise dimension and centered on the widthwise and thickness dimensions as illustrated in Figure 12. Epoxy was applied to the end regions of each bar prior to placement in the beam molds. The epoxy effectively coated the last 4 cm of each bar and was intended to prevent direct contact between the bar and the concrete in the region of the beam exposed directly to the environment.

Table 1 Concrete mixture proportions [25]

| Constituent | Description | Amount |
|-------------------|-----------------------|-------------------------|
| Cement | Type I/II | 339 kg/m ³ |
| Coarse Aggregate | Limestone | 1,017 kg/m ³ |
| Fine Aggregate | ASTM C778 Graded Sand | 678 kg/m ³ |
| Water (w/c = 0.5) | Tap Water | 169 kg/m ³ |

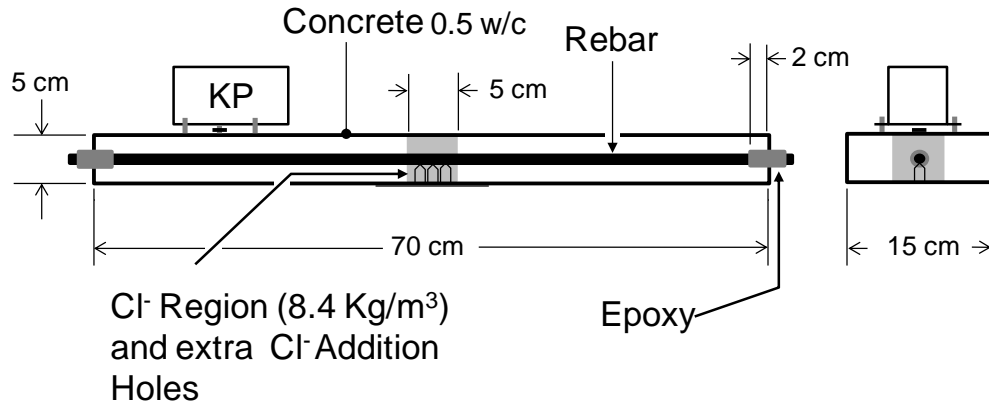


Figure 11 Test specimen dimensions and features [25].

The test plan involved measuring potential of the reinforcing steel in regions that had retained passivity and in regions undergoing active corrosion. Accordingly, the beam design provided for two inherent and distinct concrete regions: one wherein the development and sustenance of a passive film could be expected given the alkaline nature of the concrete pore water solution, and one wherein the passive film would be damaged or destroyed thus making the steel vulnerable to corrosion. As the ability of chloride ions to compromise the passive film on steel embedded in concrete has been established [3] [4], the development of two distinct regions was made possible by admixing NaCl in the small volume of concrete that was placed in the 5 x 15 x 5 cm region centered on the lengthwise midpoint of each beam as indicated in Figure 11. The contaminated region contained 13.9 kg/m^3 NaCl which equated to a chloride ion content of 8.4 kg/m^3 (2.5 wt percent of cement content), exceeding typical corrosion threshold levels [18].

The molds were made of wood and were coated lightly with oil on their inner surfaces to facilitate mold release. The beams were cast such that five of their six surfaces were macroscopically flat with roughness typical of wood form finish. The remaining surface was

hand-finished. Intermixing between the NaCl contaminated concrete and the uncontaminated concrete during molding was prevented via the use of removable dams which were placed in each mold during concrete placement and then removed immediately prior to final consolidation. This approach allowed the formation of a continuous joint between the contaminated and uncontaminated regions.

The free surfaces of the molded beams were covered immediately after final consolidation to prevent water evaporation and the beams were removed from the molds four days later. The beams were cured in plastic bags with excess water for four weeks and then left exposed to laboratory air maintained at approximately 60% relative humidity (RH) and 24°C. Open circuit potential was measured at several points on the largest beam surface (i.e. the surface opposite the free surface) using a conventional wet-tip electrode. While the potential values observed at the surface of the contaminated region of each beam indicated likelihood of corrosion [8] the difference between the average potential in the contaminated region and the average potential in the uncontaminated region was found to decrease over the course of approximately 12 weeks of ambient air exposure.

To allow a more prominent distinction between the active and passive regions to develop, the beams were moistened, enclosed in plastic bags with excess water, and subsequently modified to increase active corrosion in the contaminated region. The modification involved drilling three 1 cm diameter holes from the free surface down to the concrete immediately adjacent to the bar in the contaminated region. Each hole was partially filled with one milliliter of NaCl-saturated water and then plugged with a piece of a paper towel that had been soaked in a NaCl-saturated water solution. The drilling orientation (i.e. free surface facing upwards) was maintained for approximately 16 hours, a piece of duct tape was affixed over the holes of each

beam, and the beams were reoriented such that the largest cast surface was again facing upwards. Open circuit potential measurements made during the ensuing two weeks (the period during which the following potential stability and mapping experiments were conducted) revealed an increase in the difference in average potentials between the contaminated and uncontaminated regions to approximately 200 mV.

The same two beams were also used as test specimens in the polarization response experiments though moisture exposure conditions and accordingly, absolute observed potential values differed somewhat from those of the potential stability and mapping experiments.

2.3 Measuring Potential

Potential was measured on the replicate concrete test beam specimens using both the KP and the SCE. Although the CSE is commonly used for potential measurements, an SCE was selected as a preferred alternative in order to preclude possible measurement artifacts from CuSO_4 residue from the CSE. SCE measurements were made according to the standard practice [8] which involved pre-wetting the concrete surfaces with water. KP measurements were made on dry, undisturbed surfaces and for comparison, on surfaces pre-wetted in the same way as the SCE.

The SCE uses a fine glass frit electrolyte channel that allows only vestigial KCl contamination, while having low enough impedance to be unaffected by the FET-input front end of the data logger system used with that electrode. As indicated above, the considerations made in comparing measurements from KP and a conventional wet-tip electrode measurements are unaffected by the differences between the SCE and CSE. A 3 mm-thick sponge which was wetted with tap water (approximately 2 kOhm-cm resistivity) was placed between the SCE tip

and the concrete surface for each measurement to function as an electrical junction device as described above.

Prior to conducting the potential mapping experiments, the stability of the electrical potential value as measured by both the KP and SCE was evaluated. Evaluating the stability of the reported electrical potential value involved placing the KP on the beam in the selected location, activating the data acquisition system, and then allowing the potential to be recorded once per second for approximately three minutes. At the end of the three minute period, the KP was moved to a different location and left in place for three minutes. This was repeated until the stability record was established at each selected location. The process was then repeated with the SCE with pre-wetted surfaces as described above.

Making potential profile/map measurements with the KP in the dry surface scenario involved placing the KP on the beam in a desired starting location, activating the data acquisition protocol which recorded and averaged ten samples over the course of one second, and then subsequently moving the KP to a new location, reactivating the data acquisition protocol, and repeating until all measurements were made. The lengthwise midpoint of each beam was designated as the datum and each position along the lengthwise axis was numbered according to its location with respect to the datum. Measurements were made at 1.25 cm intervals along the cast surface of each beam and data was acquired approximately five seconds after the KP was positioned. Measuring potential with the KP in the wet surface scenario involved dabbing the concrete surface with a tap-water-soaked sponge and blotting any free surface water from the surface, waiting approximately 20 seconds, and then positioning the KP and proceeding as above.

Making potential profile/map measurements with the SCE involved the same pre-wetting regimen as in the wet surface KP scenario but differed with the rest of the procedure in that each observed potential value was allowed to stabilize prior to acquiring data. In addition, the measurement distance interval was increased to 2.5 cm to prevent pre-wetting on one spot from interfering with adjacent spots.

Wet surface repeat measurements were made after ten minutes whereas dry surface repeat measurements were made after a period of 12-16 hours of drying in ambient air. Each observed potential value was plotted as a function of its position and measurement device.

2.4 Measuring Polarization Response

The corrosion rate of a system can be estimated by evaluating the system's potential response to an impressed current. The current causes a small potential change (the polarization response) which is measured using either a conventional electrode or as detailed here, a KP. Extensive investigations have determined that within certain limitations [6] [19] [20] the ratio of potential change to impressed current density yields the polarization resistance R_p which is related to the corrosion current density i_{corr} via the Stern-Geary parameter B by the equation $i_{corr} = B/R_p$. The resulting value of i_{corr} can then be related to the corrosion rate of the steel by the usual Faradaic conversion [21] [25].

A test plan was developed to evaluate the use of the KP as a reference electrode in the measurement of polarization pulse response as in other applications [22]. Since this method, unlike potential mapping, involves measuring only relative potential changes at a single point on the concrete surface, sensitivity to spatial variations in concrete surface condition is not significant.

A small galvanostatic polarizing current was applied via an external high-impedance current source connected in series between the end of the reinforcing steel bar and a non-wetting counter electrode (CE) in direct contact with the concrete surface as illustrated in Figure 12 [6] [23]. A galvanic pulse mode was favored over a potentiostatic mode for simplicity and to eliminate the need for a potentiostatic control loop in these initial experiments.

The CE was made of a piece of flexible conductive elastomer that was able to conform to any irregularities in the concrete surface and thus maximize contact surface area. CE-to-concrete contact was enhanced by the application of a downward force provided by a pressure plate and two clamps. A hole was cut through both the pressure plate and the CE to provide KP disk access to the concrete surface. The implementation of the counter electrode and pressure plate necessitated a degree of height adjustability that the support legs of the KP used for potential profile experiments could not accommodate. Accordingly a second generation KP, hereafter referred to as the *enhanced KP*, was designed and fabricated. Implementation of the enhanced KP involved using the pressure plate as a base as indicated in Figure 12.

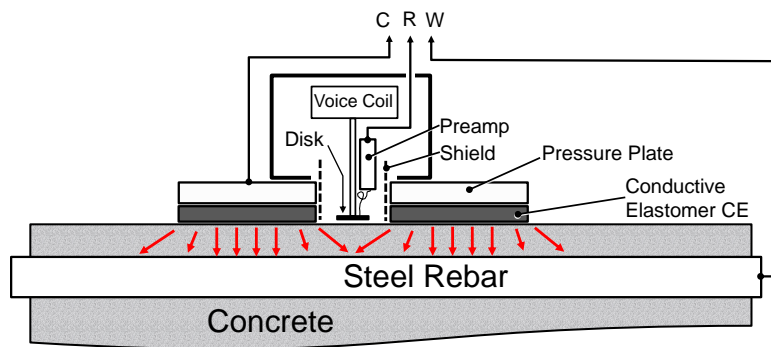


Figure 12 Schematic diagram of enhanced KP plus dry counter electrode system. Red arrows show idealized excitation current path. Note: Patent Pending.

The test plan called for polarizing the steel into the cathodic region (i.e. more negative potential) and using an amplitude that would yield deviations from the pre-pulse-application potential of approximately 15 mV. The time schedule involved monitoring the open circuit potential (OCP) for about 120 seconds, applying one galvanostatic pulse for 60 seconds, allowing the system to recover for 90 seconds, and then applying a second 60 second pulse. The potential was monitored for an additional 90 seconds after the second pulse.

Polarization response was measured first in the chloride contaminated region and then in a chloride free region 20 cm away from the lengthwise midpoint of each of the two identical beams. The probe disk was centered on the rebar in all cases. The static pre-test potential was measured with the KP at each of the test locations prior to each polarization test.

After the KP polarization tests were completed, the measurement regimen including the pre-test static potential measurement was repeated using the SCE. All tests used the same counter electrode but the SCE tests were made using a small (13x13 mm) moist sponge between the electrode and the concrete surface and no surface pre-wetting.

CHAPTER 3: RESULTS

3.1 Potential Measurement Stability

When placed on a concrete surface in a stable environment⁵, the KP almost instantaneously reported an electrical potential value that remained constant ± 1 mV throughout the observation period of approximately three minutes. Figure 13 presents the time record of electrical potential measured at four different locations on one of the beams. The minor drift in measured potential reflects a change in output relative to the value observed at $t = 0$ which corresponds to the time approximately one second after the probe was placed at the selected location. The beams had been exposed to ambient air in the laboratory for several days at the time of measurement and at least one day had passed after any surface wetting associated with SCE measurements. Primary stabilization took approximately one second, reflecting the time constant of the electronic filtering circuit.

Figure 13 also shows the electrical potential time records as measured by SCE with a wet sponge and no surface pre-wetting. As is commonly observed in such cases [8] [17], the output drifted considerably. This reflects variations in $\Delta\Phi_w^*$ and X_{BW} (Eq. 4) associated with electrolytic rearrangement in the pore network and consequent slow establishment of a new diffusion potential regime near the concrete surface as the region is infiltrated by water from the sponge. The magnitude of the drift observed in the SCE measurements (in some cases more than

⁵ Electrical potential excursions of several millivolts were observed when warm and/or moist air was blown on the sensing area. Potential values observed a few seconds after the cessation of the disturbance reflected a return to baseline conditions.

40 mV) clearly and substantially exceeded that of the KP and in most cases the potential as measured by SCE failed to stabilize by the end of the three minute observation period.

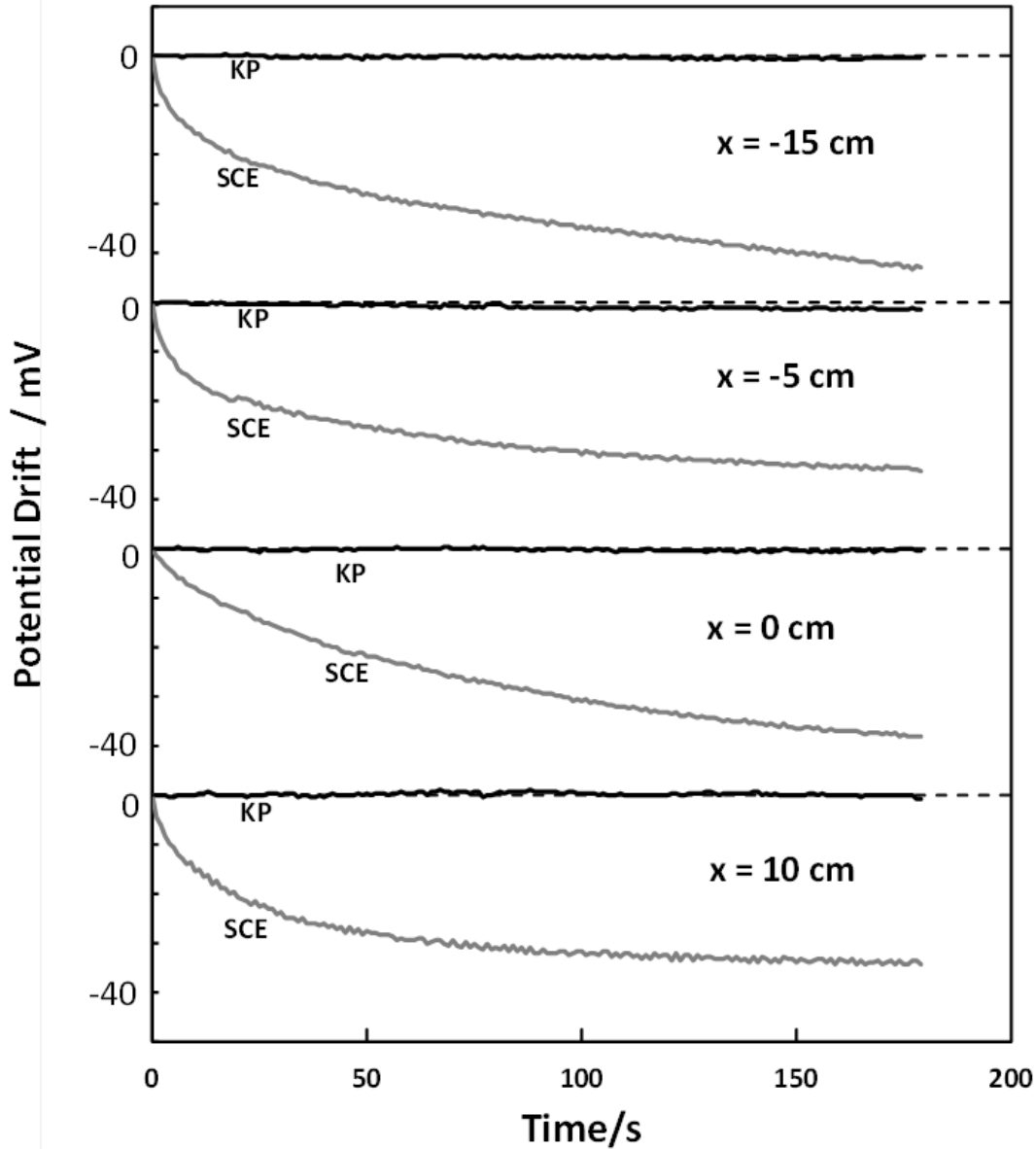


Figure 13 Stability of measured potential for KP and SCE. Potential shown as drift from value measured 1 second after probe placement on dry concrete. Results shown as stacked graphs for four positions indicated by distance from center of Beam A [25].

3.2 Effective Working Surface Position

As illustrated in Figure 10 and described by Eq.7, the electrical potential measured by the KP is the difference between the Volta potentials of the reference and working surfaces. The working surface was described previously as a small area on the outer concrete surface; thus far the terms working surface and concrete surface have been used interchangeably. For media with sufficient presence of mobile charge carriers, the working surface can indeed be said to coincide with the geometric outer surface of the material from the standpoint of the operation of a macroscopic KP [15]. For a porous material like concrete however, additional consideration must be made. Electric charge transport is dominated by the pore solution which partially fills the pore network and is normally highly conductive. The solid aggregate-cement paste matrix has properties that approach those of a porous dielectric with vestigial conductance [25].

For moist concrete, appreciable amounts of pore water are present near the concrete outer surface and thus this surface can be regarded as coincident with the working surface. The electrolyte presence in the pore network of concrete with long-term exposure to air of moderate relative humidity may be very small due to evaporation. The conductivity of the remaining electrolyte may be also significantly diminished due to reaction with atmospheric CO₂. Depending on the concrete age and external humidity those effects reach depths ranging from only a few micrometers to as much as several centimeters [6] [25].

A series of experiments was conducted to determine the extent to which the working surface coincided with the geometric outer surface for concrete in various conditions. The test plan involved making measurements at various h values on each test specimen while the KP zeroing circuit was intentionally offset from the balance condition by one volt. In this arrangement, the frequency of the main spectral component of the alternating current generated

by the probe equals the vibrating frequency and the amplitude of the current is approximately inversely proportional to h_C . The KP circuit amplifies this current and reports it as an AC potential. The RMS value of this potential was designated V_{OB} and was measured and recorded at each selected h value on each specimen. An indication of coincidence of the geometric and effective working surfaces was obtained by plotting $1/V_{OB}$ as a function of h and extrapolating the resulting curve to the h axis. The curve should intersect the h axis at $h = h_A$ if the geometric and working surfaces are coincident given that the reference surface would virtually contact the working surface with ideally unlimited output amplitude. Alternatively, the curve will intersect the h axis at a value lower than h_A if the effective working surface was deeper than the external surface.

To establish a baseline, V_{OB} was measured with the KP on a steel disk at the normal working distance of 1 mm and then subsequently measured at working distances of 1.25, 1.50, 1.75, and 2.00 mm. V_{OB} was then measured in the same fashion on each of the two beams after several weeks of exposure to ambient air in the laboratory and also on each of three other available reinforced concrete specimens that had been made for a previous investigation and had been exposed to ambient air in the laboratory for more than ten years. (The concrete compositions of these three specimens are detailed in Moreno-Sagüés [24] as mixes A, E, and F.)

The results are presented in Figure 14. The resulting values of $V_{OB}^{-1}(h)$ for the steel disk could be closely fit to a second-degree polynomial relationship with modest quadratic component [25]. The extrapolated fit function (average of two tests) intercepted the h -axis at approximately 0.56 mm reflecting good agreement with the $h_A = 0.5$ mm value expected for a metallic surface especially considering the 0.1 mm uncertainty affecting both h and h_A . The resulting values of $V_{OB}^{-1}(h)$ for each of the concrete specimens, regardless of concrete composition or age,

approximated the same shape and position of the curve for steel. Because of close superposition, variation bands that indicated the range of V_{OB}^{-1} values are shown instead of individual values [25]. The h-axis intercept of the fit for the concrete specimens was virtually the same as that for the steel surface. The greatest corresponding leftward horizontal deviation from the steel curve was only approximately 0.1 mm and was regarded as being within the overall variability range of h given the normal surface flatness deviation of the concrete specimens.

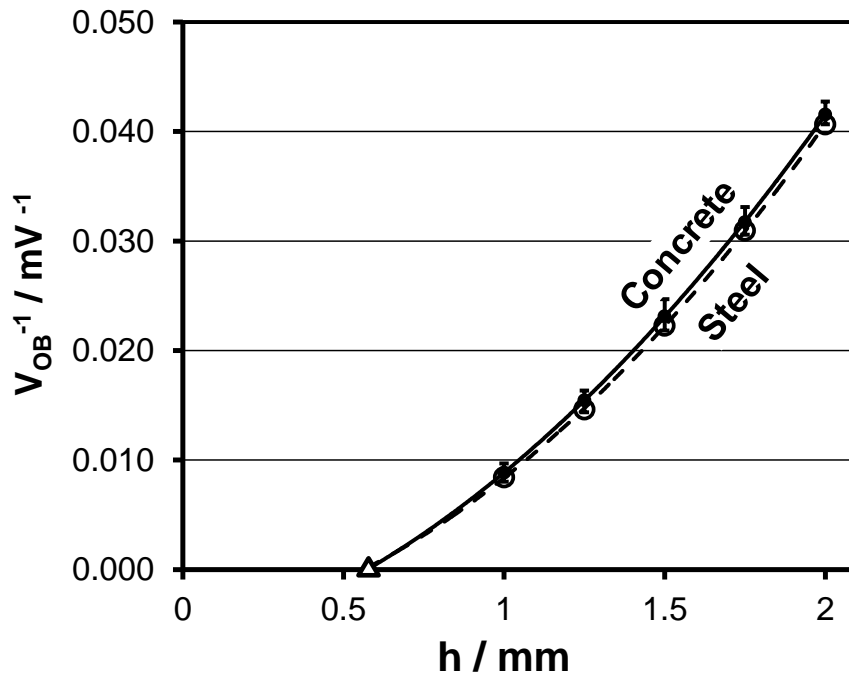


Figure 14 V_{OB}^{-1} as a function of h . Circles: Flat-machined steel surface. Range bands: Two positions on Beam A (center and 15 cm away), and three specimens aged in lab air [24]. Solid/Dashed lines: 2nd order polynomial trend fits for Steel / Concrete average. Triangle: h -axis intercepts; Steel: 0.56 mm; Concrete: 0.57 mm [25].

It was thus concluded that the concrete geometric outer surface, whether in the aged concrete specimens (subject to long term exposure to moderately dry atmospheric conditions typically associated with high (i.e. greater than 1 M Ω -cm) surface resistivity values) or the

relatively young concrete specimens, coincided with the KP working surface, at least within the level of operating position precision.

3.3 Working Distance Sensitivity

Working distance was defined as the distance between the concrete surface (i.e. working surface) and the surface of the disk (i.e. reference surface) facing the concrete surface measured when the disk was resting (i.e. not vibrating). The initial working distance value was based on the practical consideration of avoiding physical interference between the disk and the concrete surface while oscillating. The ultimate working distance was established via the methodology presented below.

As indicated above, the voice coil electromagnetic driver oscillated with an amplitude of approximately 1 mm. The resting position was the midpoint of this oscillation range and thus the minimum working distance had to be greater than one half of the disk vibrating amplitude in order to avoid contact with the concrete. As the physical constraints of the KP equipment and housing did not impose a fundamental upper limit to the height of the disk above the concrete, the maximum working distance was dictated by other factors such as capacitive effects and amplification requirements. Spurious surface and spatial charges that develop in the KP housing and supporting structure, concrete, and air in the local environment affect the electric field generated by the working surface. These charges affect the nulling potential and the effect becomes increasingly prevalent and consequential with increasing working distance [26].

This effect was quantified via an experiment that involved measuring the potential at a discrete point on the surface of one of the concrete beams, varying the working distance by placing spacers of different thicknesses between the KP adjustment screws and the concrete surface, and then measuring the resulting change in potential. As indicated in Figure 15,

increasing the working distance was found to shift the measured potential in the positive direction from a negligible amount to a value less than 40 mV when increasing h from 1 mm to 2 mm, a change much greater than the usual variability of h . The shift was an approximate linear function of the increase in working distance and was found to be on the same order of magnitude when measured at different locations on the concrete surface and on a flat-machined smooth steel plate. The actual magnitude of the shift was found to depend on the recent maintenance and cleaning history of the disk, its supporting assembly, and housing [25].

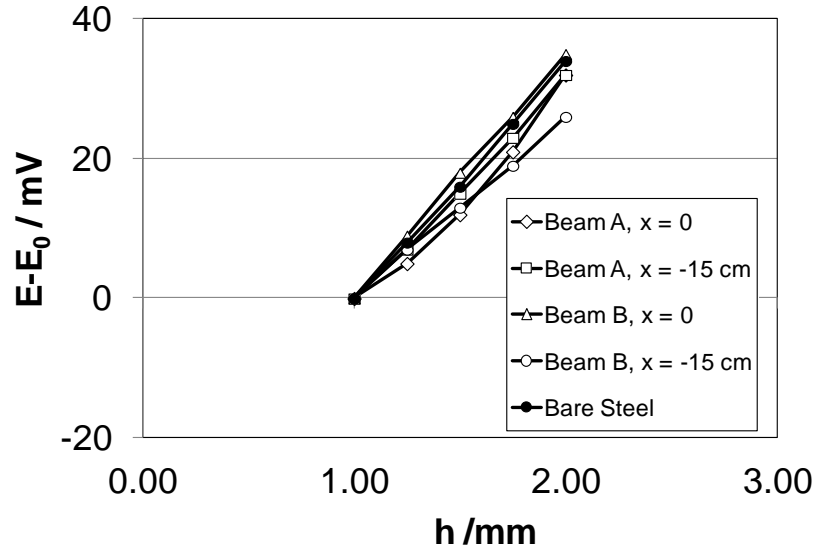


Figure 15 Change in potential as a function of working distance.

3.4 Application: Potential Profile Mapping

Figure 16 presents potential profiles obtained by measuring electrical potential at specific lengthwise intervals along the top surface of each of the duplicate beam specimens using the KP and the SCE. As described in the Methods section, potential was measured along the lengthwise axis of the selected beam with the KP under dry surface conditions. After recording the potential

at each point, the measurement regimen was immediately repeated without making any changes to the system. The individual test spots on the surface of the beam were then moistened with tap water and potential at each point was measured with the wet sponge tipped SCE. As in the case of the KP, the measurement regimen was immediately repeated. The individual test spots were remoistened and the potential at each point was once again measured with the KP and then re-measured. The duplicate results for the three sets of measurements were labeled KP-Dry, SCE Wet and KP-Wet respectively in Figure 16. The results from both beams were comparable within the variability levels commonly encountered with assessing corrosion phenomena in concrete [25].

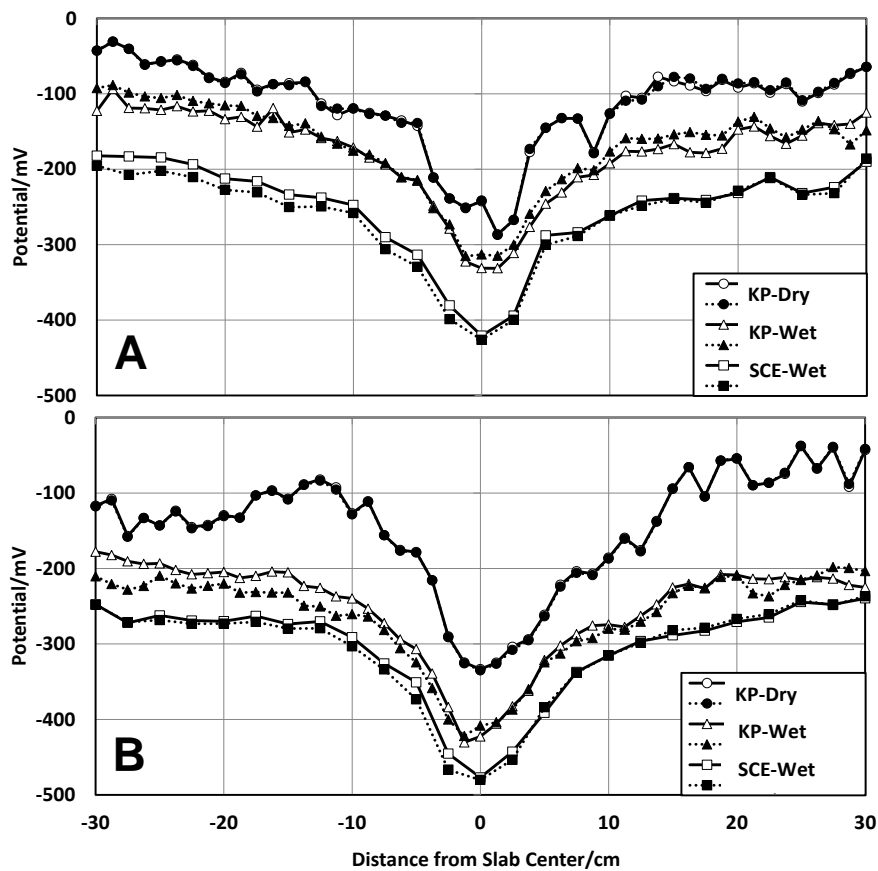


Figure 16 Potential profiles associated with steel in concrete beams A and B [25].

Each SCE profile showed a distinct negative dip pattern of approximately 200 mV deep that would typically be expected in a concrete beam with a centrally corroding segment on a longitudinal reinforcing bar [27] [28]. As illustrated in Figure 16, the KP profile shapes and ranges generally reproduced the SCE profile patterns under both dry and wet surface conditions.

3.4.1 Short Term Repeatability

The KP-Dry data showed closely overlapping consecutive profiles along the entire length of the specimen, consistent with the nearly constant output noted in Figure 13 for the KP placed on a stabilized dry concrete surface.

The SCE-Wet data showed greater variability in consecutive results than those for KP-Dry data, reflecting spot-to-spot variations in time-dependent water absorption and evaporation following the pre-wetting. The changes, which can be interpreted as noted earlier in the context of Eq.4, were in the same order as those shown in the time charts in Figure 13 for the SCE data after the same approximate time period (i.e. one minute) after placing the wet sponge on a previously dry concrete surface.

The KP-Wet data showed greater variability than the KP-Dry data and similar variability to the SCE-Wet data. The variability is again attributed to time evolution of moisture on the concrete surface and the moisture's affect on X_{AW} and $\Delta\Phi_W$ in Eq. 8. In addition, some amount of variability may be attributed to the influence of minute changes in the amount of water adsorbed on the reference disk surface following evaporation from the concrete surface as noted previously.

3.4.2 Profile Correlation

The graphs in Figure 17 show linear correspondence between potentials measured by KP (under both dry and wet surface conditions) and potentials measured by SCE. The slopes range from 0.87 to 1.12 and correlation coefficients ranging from 0.87 to 0.96. The corresponding offsets from an ideal 1:1 coincidence with the CSE readings were about +100 to +200 mV for the KP-Dry condition, and approximately half of that amount for the KP-Wet condition.

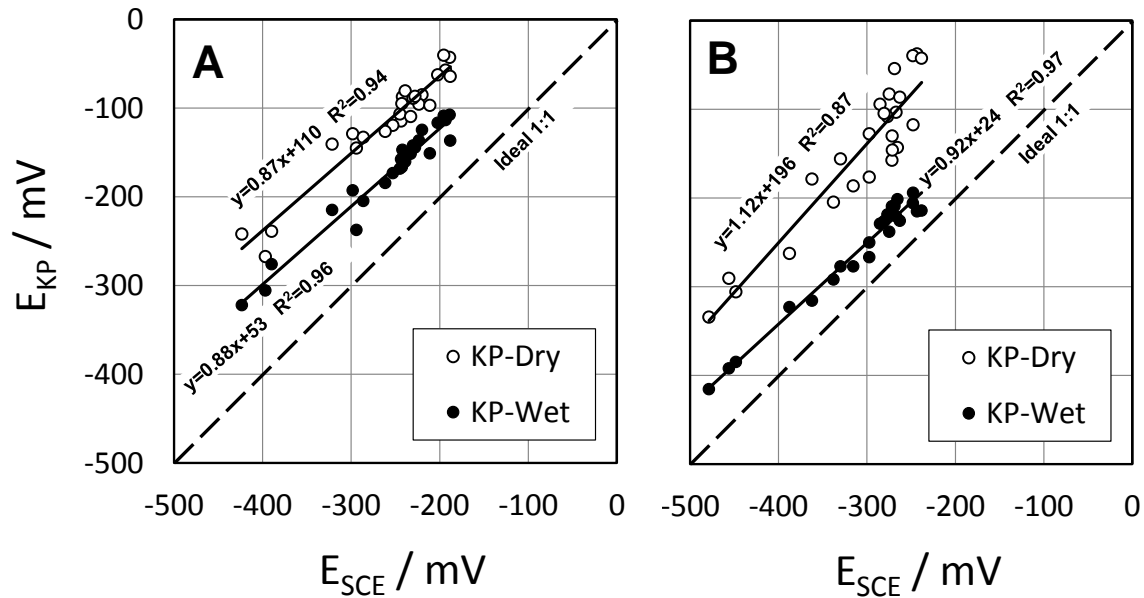


Figure 17 Linear correspondence between KP and SCE potential measurement values [25].

Comparison of the profiles is conceptually more straightforward for the wet surface cases, where both the KP and the SCE interacted with a concrete surface in the same nominal condition and at a similar measurement rate. In the case of a correlation slope of unity, the potential offset of the KP-Wet values from the SCE values could be viewed as a temporary calibration for the KP measurement values with respect to potential measurements in the SCE

scale. This calibration would correspond ideally to the addition of the terms in first set of square brackets in the equivalent of Eq. 9 for an SCE [25]. Even if the timing of the measurements with respect to the moment of wetting was strictly controlled, the calibration should be viewed as temporal given day to day variations in environmental variables and the effects of long term evolution of the concrete surface on the parameters in Eq. 8, particularly X_{AR} , which is very sensitive to the makeup of a region only a few atomic distances thick on the disk surface [25].

Monolayer-levels of moisture or organic vapor precipitation can readily develop given exposure to normal environmental conditions and can cause potential changes greater than 100 mV [13]. Variations of that order were noted during tests conducted at different times particularly if the KP disk had been recently cleaned.

3.4.3 KP-Dry Profile Offset

As illustrated in Figure 16 and Figure 17, the KP-Dry profiles were positively offset with respect to those obtained in the wet condition. This offset is consistent with the less negative potential values reported by the KP as presented in Figure 13 both when the concrete surface was only beginning to depart from its initial dry condition and when the surface had been subject to substantial water absorption from the sponge.

The change can be attributed to the slow dissipation of a diffusion potential (manifested in the combined values of X_{BW} and $\Delta\Phi^*_W$ or X_{AW} and $\Delta\Phi_W$ in Eq.4 or 8 respectively) due in part to a gradient in OH^- concentration in the water partially filling the pores [17] [29]. The OH^- concentration of the pore water is relatively higher deeper inside the concrete, due to alkali content [30], and smaller near the surface because of carbonation by interaction with atmospheric CO_2 .

In this interpretation, the higher diffusivity of the OH^- ions compared with that of the balancing cations [29] promotes a diffusion potential difference where the outer surface is more negative than the inside. Because of the polarity of the KP and SCE measurements, this results in a potential reading that is more positive than it would be in the absence of the diffusion potential.

Other electrolytes, such as those associated with chloride salts, would have additional individual effects. As water refills the partially empty pore network near the surface, the resulting enhanced transport between outer and inner regions lessens solute concentration gradients and thus reduces the magnitude of the junction potential difference and results in a shift of the measured potential in the negative direction.

It should also be noted that the potential offset depends on the nature of the KP disk material. A gold-plated disk, for example, would have yielded a different relative profile position than the stainless steel disk used in these experiments.

3.4.4 Spatial Variability of Observed Potential Values

The KP-Dry surface profiles showed more vertical spatial variability than those in the wet condition. Given the high repeatability noted above, the spatial variability can be said to represent true local potential differences on dry regions 1.25 cm apart. (The source of the short distance variability was not identified and should be the subject of future study.) Given the lower short-distance spatial variability of the KP-Wet profiles, it may be proposed that the local variations in the dry case are associated with variations in diffusion potential related to local differences in the degree of carbonation, or differences in the evaporative concentration of other species at the extreme outer surface. Some of the differences may be associated with the local proximity to the surface of the coarse aggregate. Those effects would diminish with pre-wetting

as discussed earlier, resulting in the observed smoother potential profile than that in the dry condition [25].

3.4.5 Concrete Moisture Condition

The moisture condition of the steel-concrete interface was generally considered to be unchanged while switching between the dry and wet conditions of the outer concrete surface over short periods of time. Any possible changes were considered to be negligible because the concrete beams were relatively young and in addition had been periodically conditioned with moisture. Under these conditions and with consideration of the 0.5 water to cement (w/c) ratio, convective transport is expected to be limited to a depth (from the surface) appreciably less than the concrete cover thickness [31]. Transport by diffusion through the pore network of the concrete is very slow and it would also not be expected to lead to any noticeable effects in the time scale considered [6].

Differences in the results from the dry and wet surface experiments were accordingly attributed to moisture-related changes in the regions closer to the outer concrete surface. It is noted that the moisture content at the rebar surface could however change substantially given external moisture cycling if cover was shallower or the cycles longer. In such cases the potential difference between the two conditions observed with the KP could also include a component associated with variations in the potential across the metal-pore water interface, not unlike those encountered between immersed and emersed conditions in passive metals [32].

It should be noted that the profile measurements specifically apply to cases that involve strongly defined corrosion macrocell patterns that dominate the potential distribution on the concrete. The partial contribution resulting from the chloride content gradient, which can also

indirectly affect the local rate of carbonation, should be further investigated. Development of a rational calibration procedure to relate the potential determined by the KP to that of the metal-concrete interface (perhaps by adequate choice of an external concrete surface condition and a methodology comparable to that of Leng [16]) is also regarded as an important element of future work.

3.5 Application: Polarization Response Measurement

3.5.1 Baseline Potential Measurements

Table 2 lists the potential values measured with the enhanced KP and counter electrode system placed on each beam at its respective lengthwise midpoint and at a point 20 cm distant. In each case the steel potential with respect to the concrete surface in the chloride contaminated central region was substantially more negative than the potential in the passive region, consistent with the results presented above. Table 2 also shows the potentials measured using a conventional SCE in both regions. As in the case of the basic KP described above, KP potentials are effectively offset from SCE potentials by an approximately constant amount. The potential difference ΔE between the active and passive regions of each beam was also approximately constant. These observations effectively confirmed that the enhanced KP was operating in a way consistent with the basic KP.

Table 2 Baseline potential measurements

| | Beam A | | Beam B | |
|---|-----------------|---------------------|-----------------|-----------------------|
| | Active (x=0) | Passive (x=20cm) | Active (x=0) | Passive (x = 20cm) |
| Open Circuit Potential, KP [mV] | -408 | -207 | -314 | -189 |
| Open Circuit Potential, SCE [mV] | -369 | -158 | -294 | -175 |
| ΔE, KP [mV] | 201 | | 125 | |
| ΔE, SCE [mV] | 211 | | 119 | |

3.5.2 Dynamic Polarization Measurements

The KP measured polarization response by tracking the potential evolution in real time. Random fluctuations (“noise”) in the measured potential typically stayed well below 1 mV and this effective resolution was adequate to establish a clear system response given that the impressed potential deviations were on the order of several millivolts, which is the customary potential excursion range in polarization resistance or electrochemical impedance evaluations in concrete [3] [4].

Figure 18 (left side) shows the response to the galvanostatic pulses as measured with the KP. The system behaved as expected with an initial instantaneous change reflecting the effective ohmic potential drop across the solution resistance between the concrete surface and the underlying rebar. This was followed by a slower potential evolution, part of which consisted of the current satisfying the quasi-capacitive demand of the effective interfacial charge storage process and the rest consisting of the current polarizing the electrochemical Faradaic reactions of the interface.

On first approximation, the overall behavior may then be represented by that of a solution resistance R_s in series with the parallel combination of an interfacial non-ideal capacitance represented by a constant phase element (CPE) and a polarization resistance, R_p [33]. The

corresponding analog circuit is presented in Figure 19. The analog circuit responds in the time domain in a manner that essentially replicates the observed response illustrated in Figure 18.

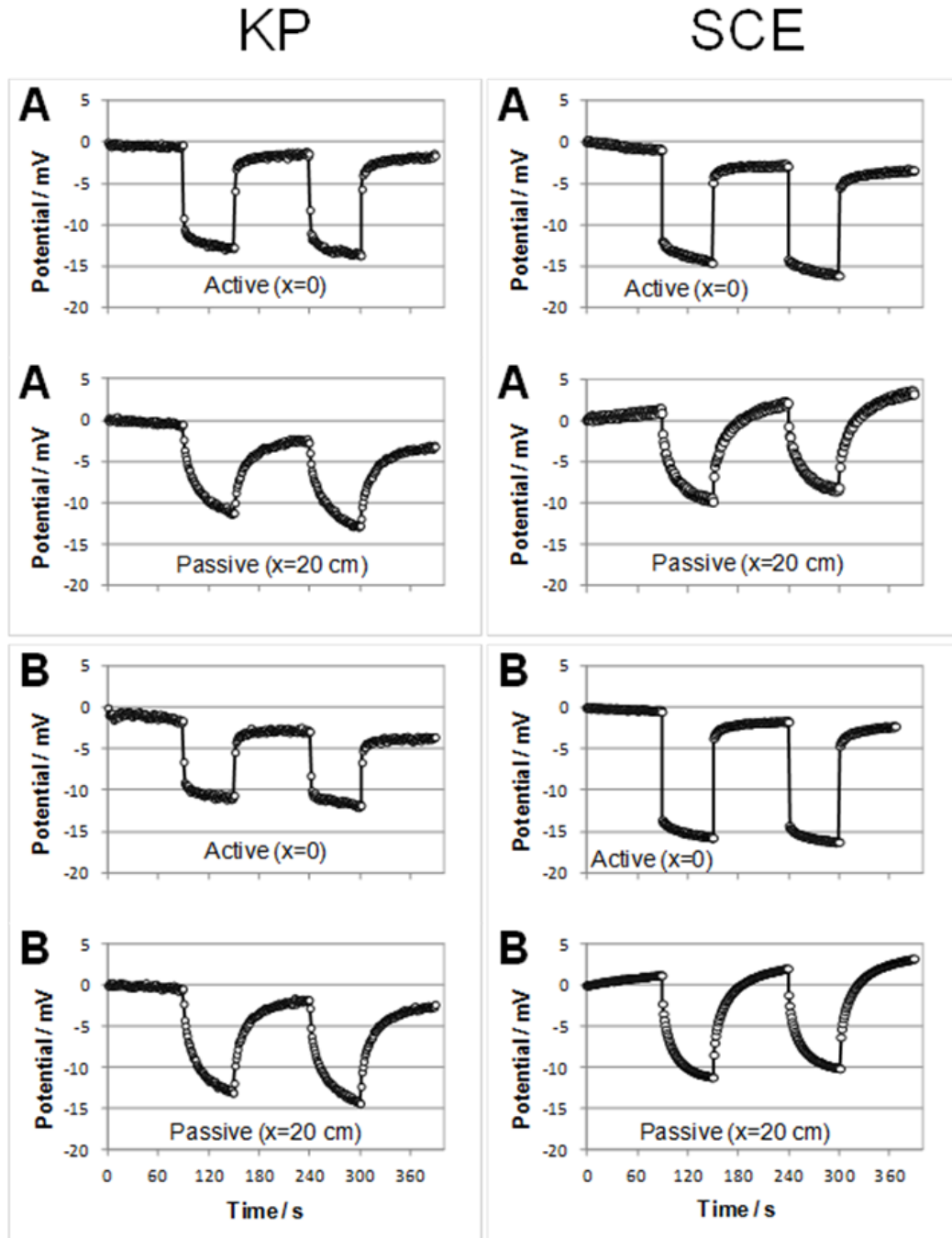


Figure 18 System response to Galvanostatic pulses as measured by KP and SCE. Note that the center regions (i.e. $x=0$) of beams A and B contain actively corroding steel while other regions (e.g. $x=20$ cm) contain steel in the passive state. All potentials have been normalized to represent deviations from the starting condition.

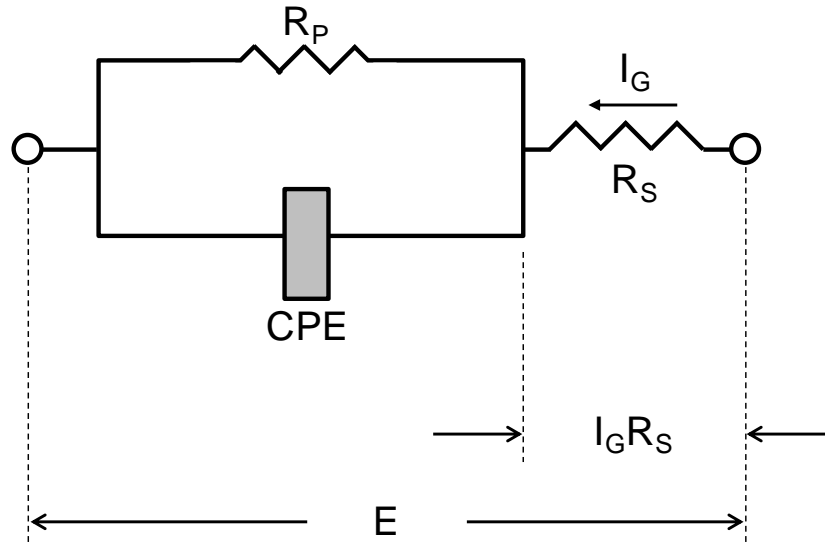


Figure 19 Analog circuit corresponding to corroding system. [33]

As illustrated in Figure 18, the response observed in each of the two replicate beams was comparable, demonstrating consistent outcome of the methodology when switching specimens. In each beam, the response to the second galvanostatic pulse closely replicated that of the first, showing good immediate reproducibility of results. The slight offset in the second pulse compared with the first pulse came as a consequence of the relatively short recovery time between the pulses indicating incomplete stabilization of the system before the second pulse. Correspondingly, the length of the pulse (60 seconds) allows for only partial evolution of the system toward a terminal state wherein the interface would act as the simple series combination

$$R_T = R_s + R_p \quad \text{Eq. 10}$$

where R_T is the total resistance. By ignoring this residual effect a nominal result may be obtained by evaluating

$$R_T \approx - (E_f - E_i) / I_g \quad \text{Eq. 11}$$

where E_f and E_i are the values of the potential recorded just before and at the end of the applied galvanic pulse. Following the same approach used in instant-off solution resistance compensation procedures, [34] a nominal value of R_p may likewise be obtained by evaluating

$$R_p \approx - (E_f - E_{i0}) / I_g \quad \text{Eq. 12}$$

where E_{i0} is the value of the instant potential obtained immediately following the beginning of the pulse application. In the present introductory tests, E_{i0} was taken to be the potential measured 2 seconds after starting application of the pulse.

Table 3 shows the selected values of I_g and the resulting values of E_i , E_{i0} , E_f , R_T , R_p , and R_s (by difference) for each of the beams and at each of the two locations examined. Analysis only involved the results of the first pulse. Any residual potential drift was de-trended by calculating the corresponding linear baseline trend and subtracting from the data. The results are consistent with the appearance of the potential traces in Figure 18, whereby the value of R_p is much smaller at the central active steel locations in accordance with the expectation of high local corrosion rate (and with the more negative static potential noted earlier), while R_p is relatively higher at the $x = 20$ cm, passive steel position. The observed values of R_s were not very different between the active and passive steel positions. This was consistent with expectations, given that the concrete pore water is highly conductive due to its high ionic content even in the absence of chloride ions, and the fact that introduction of chloride ions in moderate amounts as used here does not create a radical relative increase in conductivity.

Comparable tests were conducted with the SCE and the results of these tests were compared with those of the KP. The SCE results, displayed on the right side of Figure 18, show excellent qualitative and general quantitative agreement with the KP results. As was observed in the potential mapping experiments, the potential values measured with the SCE were much more prone to drift than those the KP. Resistive parameters for the circuit in Figure 19 were calculated

in the same way as those for the KP and the results are presented in Table 3. Graphic comparison of the R_T and R_s values obtained with both methods, presented in Figure 20, illustrates general consistency thus validating the functional capability of the KP in measuring polarization response.

Table 3: Summary of dynamic polarization measurements

| | Beam A | | | | Beam B | | | |
|--------------------|--------------|------------------|--------------|------------------|--------------|------------------|--------------|------------------|
| | KP | | SCE | | KP | | SCE | |
| | Active (x=0) | Passive (x=20cm) | Active (x=0) | Passive (x=20cm) | Active (x=0) | Passive (x=20cm) | Active (x=0) | Passive (x=20cm) |
| I_g [μ A] | 39.7 | 7.7 | 39.0 | 7.6 | 39.6 | 7.9 | 37.5 | 7.7 |
| E_i [V] | -2.62E-04 | 5.44E-05 | -1.84E-04 | 2.51E-04 | 1.28E-04 | -1.12E-05 | 1.16E-04 | 1.22E-04 |
| E_{io} [V] | 9.97E-03 | 3.18E-03 | 1.09E-02 | 3.71E-03 | 7.60E-03 | 3.80E-03 | 1.35E-02 | 4.81E-03 |
| E_f [V] | 1.19E-02 | 1.05E-02 | 1.25E-02 | 1.13E-02 | 8.92E-03 | 1.20E-02 | 1.50E-02 | 1.32E-02 |
| R_T [Ω] | 305 | 1,351 | 324 | 1,451 | 222 | 1,514 | 396 | 1,701 |
| R_p [Ω] | 47 | 945 | 39 | 995 | 33 | 1,032 | 39 | 1,092 |
| R_s [Ω] | 258 | 406 | 285 | 455 | 189 | 482 | 357 | 609 |

Note: The E_i and E_{io} values contained in the table represent deviations from an arbitrarily zeroed condition for instrumentation purposes. Actual E_i values are presented in Table 2.

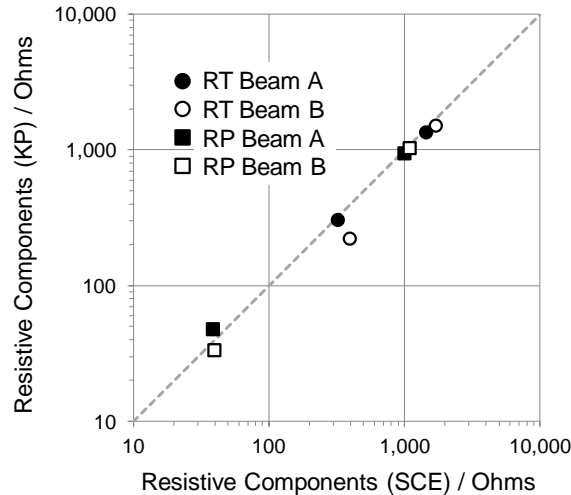


Figure 20 Comparison between KP and SCE galvanostatic pulse polarization results. Data from Table 3 shows general agreement between results. The dashed line represents theoretical 1:1 correlation.

CHAPTER 4: COMMENTS

The current work demonstrated the practical feasibility of using a KP to measure electrical potential of steel embedded in concrete on the surface of the concrete. The KP provided exceptionally stable values on dry concrete surfaces and maintained sufficient measurement sensitivity for detailed potential mapping and polarization response analysis. The KP is particularly attractive as a means by which potential measurements can be made given its ability to make practically instantaneous and non-intrusive measurements and the fact that it requires neither direct contact with the surface nor prior surface preparation in the form of wetting and post-wetting stabilization. The measurements showed high repeatability. Sensitivity to working distance was modest and thus exact control of the distance is not a critical issue.

The present work supports the concept of using a KP as an alternative to conventional wet-tip electrodes in making potential surveys of bridge decks and similar structures. This application would benefit from the KP's speed and ease of use, stability, ability to operate without contacting the concrete surface, and the loss of the need for laborious maintenance of wet contacts [8] [9]. The KP or an array of multiple KPs may be particularly suitable for adaptation to automatic operation that could involve trailing behind a slow moving vehicle which could prove less disruptive to roadway traffic than conventional methods.

Further development in this particular application would necessitate consideration of scatter that would likely be introduced by probe and concrete surface conditions especially given the possible presence of contaminant spills and other common alterations of the structural surface. Some of the scatter, as well as sensitivity to surface roughness, might possibly be

reduced by using a larger reference disk and a higher disk-to-surface distance [25].

Modifications of this sort could provide for spatial averaging of the output with consequent filtering of short-distance variations. It is believed that the existing KP could be readily scaled using available technology.

In addition, the probe in its current form would require a ground contact to one point in the normally electrically continuous reinforcing steel assembly of the structure to be assessed. In the case of a trailer-mounted probe or probe array, that connection would be implemented beforehand with a flexible and temporary extension cable. Alternatively corroding spots could be identified without using a ground contact by implementing the KP in a “relative potential” mode, if the surface potential gradient is large enough. In this case a stationary wet-tip reference electrode could be used if both it and the underlying concrete have sufficiently low impedance to keep electrical noise at acceptable levels. It should be noted that the feasibility of this approach has yet to be established by conceptual development and demonstration.

The dynamic polarization tests described above were conducted in a Galvanostatic mode that involved the use of trial and error to select a current value that did not result in excessive potential excursion. The galvanostatic measurement technique was chosen as a convenient means to establish the capability of the KP and it should be noted that there is no fundamental limitation of application of the KP to measuring polarization of steel in concrete by other methods, such as those that rely on automatic potential control. Initial tests with a full control loop for potential and current using a commercial potentiostat such as those commonly used for linear polarization resistance or electrochemical impedance spectroscopy have been performed with promising performance and will be reported in future publications.

It is noted for clarity that the use of the KP as addressed here obviates the need for direct contact with the concrete surface at the potential test point. A new technique that involves using polarization measurements to assess corrosion with current injection and extraction points with contacts on the concrete surface has been introduced elsewhere [35] but it addresses a different issue not to be confused with that of this thesis. It is further noted that it may be possible in the future to favorably combine aspects of each.

The high sensitivity of the KP to the disk and concrete surface conditions indeed constitutes a possible source of scatter but simultaneously offers a powerful alternative to investigate phenomena in which a wet-tip electrode would be too disruptive. Among other applications, the KP with appropriate customization may be adaptable for applications that seek to [25]:

- (i) Measure the evolution of the early stages of concrete carbonation in real time by monitoring the associated diffusion potential development, a sensitivity that applies also to the following.
- (ii) Detect moisture content gradients that would have been otherwise overwhelmed by contact with a wet electrode tip.
- (iii) Detect diffusional penetration and partition of moisture and chemical species such as chloride ions between aggregate and hydrated cement paste in concrete cross sections.
- (iv) Assess the transport and distribution of migrating corrosion inhibitors in concrete; (v) characterize the penetration and aging of concrete surface treatments such as silane/siloxane compounds.
- (v) Characterize the extent of evaporative concentration of species such as chloride ions on the external concrete surface.

- (vi) Make assessments of sulfate attack.
- (vii) Assess the degree of concrete surface contamination and the effectiveness of cleaning and remediation methods.
- (viii) Assess depolarization performance of cathodic protection systems.

CHAPTER 5: CONCLUSIONS

- The practical operation of a macroscopic Kelvin Probe (KP) for contactless measurement of concrete surface potentials and polarization resistance of reinforcing steel in concrete without contacting the concrete surface was successfully demonstrated. Results in all cases were in good agreement with results of similar tests conducted with a conventional reference electrode.
- The KP provided nearly instantaneous and highly stable potential values on dry concrete surfaces, in contrast with conventional wet-tip electrodes which experience considerable potential drift upon placement on the same surfaces.
- The observed potential values were found to be associated with a plane surface closely approaching the outer concrete surface in all cases including those of specimens that had been exposed to dry and naturally carbonating lab air for many years, for which high surface resistivity is expected.
- The KP output was only modestly sensitive to changes in the reference disk to concrete surface working distance.
- The shape and range of potential profiles measured with the KP were consistent with the location of the local anode in a reinforced concrete beam with a well-differentiated centrally corroding rebar segment. The KP profiles were offset from, but comparable in shape and range, to those obtained independently with a conventional wet-tip reference electrode. The offset depended on the condition of both the KP disk and the concrete

surface, so appropriate calibration is needed if absolute potential determination with the KP is desired.

- Comparable KP profile features were obtained when sampling the concrete in either the dry or a pre-wetted surface condition, but with greater point-to-point variability in the former. The variability reflects the sensitivity of the KP output to the local condition of the concrete surface. That sensitivity may be caused by the development of ionic concentration gradients with depth from the concrete surface, with associated diffusion potential differences [25].
- The results encourage exploration of the use of the KP for fast automated field corrosion potential surveys, precise polarization and electrochemical impedance determination in dry concrete surfaces, and physicochemical determinations in concrete for conditions where the use of a conventional wet-tip reference electrode would be disruptive.

REFERENCES

- [1] S. K. Lee, "Current State of Bridge Deterioration in the U.S. - Part 1," *Materials Performance*, vol. 51, pp. 62-67, Jan. 2012.
- [2] A.A. Sagüés, *Class Notes, Structural Life Prediction*. University of South Florida Course CGN 6933 Sec.901, CRN: 83180, 2011.
- [3] P. Gellings, *Introduction to Corrosion Prevention and Control*. Enschede, Netherlands: University of Twente, 2005.
- [4] M. Fontana, *Corrosion Engineering, third edition*. New York, NY: McGraw-Hill, 1987.
- [5] U.M. Angst, B. Elsener, C.L. Larsen, O. Vennesland, "Chloride Induced Reinforcement Corrosion: Electrochemical Monitoring of Initiation Stage and Chloride Threshold Value," *Corrosion Science*, vol. 53, pp. 1451-1464, 2011.
- [6] L. Bertolini, B. Elsener, P. Pedferri, R. Polder, *Corrosion of Steel in Concrete*. Weinheim, Germany: Wiley, 2004.
- [7] Y. Schiegg, M. Buchler, and M. Brem, "Potential Mapping Techniques for the Detection of Corrosion in Reinforced Concrete Structures: Investigation of Parameters Influencing the Measurement and Determination of the Reliability of the Method," *Materials and Corrosion*, vol. 60, pp. 79-86, 2009.
- [8] ASTM C876-09, "Standard Test Method for Half-Cell Potentials of Uncoated Reinforcing Steel in Concrete," West Conshohocken, PA: ASTM 2009.
- [9] B. Elsener, C. Andrade, J. Gulikers, R. Polder, and M. Raupach, "Half-Cell Potential Measurements-Potential Mapping on Reinforced Concrete Structures," *Materials and Structures*, vol. 36, pp. 461-471, 2003.
- [10] J. Bockris, A. Reddy, *Modern Electrochemistry, Vol. 2*. New York, NY: Plenum Press, 1970.
- [11] U. Angst, O. Vennesland, R. Myrdal, "Diffusion Potentials as Source of Error in Electrochemical Measurements in Concrete," *Materials and Structures*, vol. 42, pp. 365-375, 2009.

- [12] U. Angst, B. Elsener, R. Myrdal, O. Vennesland, "Diffusion Potentials in Porous Mortar in a Moisture State Below Saturation," *Electrochimica Acta*, vol. 55, pp. 8545-8555, 2010.
- [13] U. Klein, W. Vollmann, P.J. Abatti, "Contact Potential Differences Measurement: Short History and Experimental Setup for Classroom Demonstration," *IEEE Transactions on Education*, vol. 46, pp. 338-344, 2003.
- [14] M. Stratmann, H. Stachel, "On the Atmospheric Corrosion of Metals which are Covered with Thin Electrolyte Layers-I. Verification of the Experimental Technique," *Corrosion Science*, vol. 30, pp. 681-696, 1990.
- [15] L. Kronik, Y. Shapira, "Surface Photovoltage Phenomena: Theory, Experiment, and Applications," *Surface Science Reports*, vol. 37, pp. 1-206, 1999.
- [16] A. Leng, H. Streckel, M. Stratmann, "The Delamination of Polymeric Coatings from Steel- Part 1. Calibration of the Kelvinprobe and Basic Delamination Mechanism," *Corrosion Science*, vol. 41, pp. 547-578, 1999.
- [17] Myrdal, R., "Phenomena that Disturb the Measurement of Potentials in Concrete," *Corrosion/96*, paper no. 339, NACE International, Houston, 1996.
- [18] K.Y. Ann, H.W. Song, "Chloride Threshold Level for Corrosion of Steel in Concrete," *Corrosion Science*, vol. 49, pp. 4113-4133, 2007.
- [19] C. Andrade, J. Gonzalez, "Quantitative Measurements of Corrosion Rate of Reinforcing Steels Embedded in Concrete Using Polarization Resistance Measurements," *Werkstoffe und Korrosion*, vol. 29, pp. 515-519, 1978.
- [20] A.A. Sagüés, M.A. Pech-Canul, S. Al-Mansur, "Corrosion Macrocell Behavior of Reinforcing Steel in Partially Submerged Concrete Columns," *Corrosion Science*, vol. 45, pp. 7-32, 2003.
- [21] D. Jones, *Principles and Prevention of Corrosion, 2nd ed.* Upper Saddle River, NJ: Prentice Hall, 1995.
- [22] G.S. Frankel, M. Stratmann, M. Rohwerder, A. Michalik, J. Dora, M. Wicinski, "Potential Control under Thin Aqueous Layers using a Kelvin Probe," *Corrosion Science*, vol. 49, pp. 2021-2036, 2007.
- [23] M.A. Pech-Canul, A.A. Sagüés, P. Castro, "Influence of Counter Electrode Positioning on Solution Resistance in Impedance Measurements of Reinforced Concrete," *Corrosion*, vol. 54, pp. 663-667, 1998.



- [24] E.I. Moreno, A.A. Sagüés, R.G. Powers, "Performance of Plain and Galvanized Reinforcing Steel During the Initiation Stage of Corrosion in Concrete with Pozzolanic Additions," *Corrosion/96*, paper no. 326, NACE International, Houston, 1996.
- [25] A.A. Sagüés and M.T. Walsh, "Kelvin Probe Electrode for Contactless Potential Measurement on Concrete-Properties and Corrosion Profiling Application," *Corrosion Science*, vol. 56, pp. 26-35, 2012.
- [26] B. Ritty, F. Wachtel, R. Manquenouille, F. Ott, J. Donnet, "Conditions Necessary to get Meaningful Measurements from the Kelvin Method," *J. Phys. E: Sci. Instrum.*, vol. 15, pp. 310-317, 1982.
- [27] S.C. Kranc, A.A. Sagüés, "Detailed Modeling of Corrosion Macrocells on Steel Reinforcing in Concrete," *Corrosion Science*, vol. 43, pp. 1355-1372, 2001.
- [28] J. Ozbolt, G. Balabanic, M. Kuster, "3D Numerical Modeling of Steel Corrosion in Concrete Structures," *Corrosion Science*, vol. 53, pp. 4166-4177, 2011.
- [29] Myrdal, R., "Potential Gradients in Concrete Caused by Charge Separations in a Complex Electrolyte," *Corrosion/97*, paper no. 278, NACE International, Houston, 1997.
- [30] L. Cáseres, A.A. Sagüés, S.C. Kranc, R.E. Weyers, "In-situ Leaching Method for Determination of Chloride in Concrete Pore Water," *Cement and Concrete Research*, vol. 36, pp. 492-503, 2006.
- [31] P. Schiessl, S. Lay, *Corrosion in Reinforced Concrete Structures*, H. Boehni, Ed., Cambridge: CRC Press, Woodhead Publishing Ltd., 2005, pp. 91-134.
- [32] R. Hausbrand, M. Stratmann, R. Rohwerder, "The Physical Meaning of Electrode Potentials at Metal Surfaces and Polymer/Metal Interfaces: Consequences for Delamination," *Journal of the Electrochemical Society*, vol. 155, pp. C369-C379, 2008.
- [33] A. Sagüés, S. Kranc, E. Moreno, "Evaluation of Electrical Impedance with Constant Phase Angle Component from the Galvanostatic Step Response of Steel in Concrete," *Electrochimica Acta*, vol. 41, no. 7/8, pp. 1239-1243, 1996.
- [34] H. Hack, P. Moran, J. Scully, "The Measurement and Correction of Electrolyte Resistance in Electrochemical Tests," ASTM, Philadelphia, 1990.
- [35] C. Andrade, I. Martinez, M. Castellote, "Feasibility of Determining Corrosion Rates by means of Stray Current-induced Polarization," *Journal of Applied Electrochemistry*, vol. 38, pp. 1467-1476, 2008.

APPENDICES

Appendix A Permission for Use of Table and Figures

The subject license applies to Table 1, Figure 1, Figure 2, Figure 3, Figure 4, Figure 5, Figure 6, Figure 7, and Figure 8.

To ensure that you continue to receive our emails,
please add rightslink@marketing.copyright.com to your [address book](#).



Thank You For Your Order!

Dear Michael Walsh,

Thank you for placing your order through Copyright Clearance Center's RightsLink service. Elsevier has partnered with RightsLink to license its content. This notice is a confirmation that your order was successful.

Your order details and publisher terms and conditions are available by clicking the link below:
<http://s100.copyright.com/CustomerAdmin/PLF.jsp?ref=9938ab83-696d-4ba9-9fb7-8b0b0baa3ff3>



Order Details

Licensee: Michael T Walsh
License Date: Nov 6, 2013
License Number: 3263120866226
Publication: Corrosion Science
Title: Kelvin Probe electrode for contactless potential measurement on concrete - Properties and corrosion profiling application
Type Of Use: reuse in a thesis/dissertation
Total: 0.00 USD

Appendix B Permission for Use of Excerpts

Excerpts from Sagüés and Walsh, "Kelvin Probe Electrode for Contactless Potential Measurement on Concrete-Properties and Corrosion Profiling Application," *Corrosion Science*, vol. 56, are indicated in text.

To ensure that you continue to receive our emails,
please add rightslink@marketing.copyright.com to your [address book](#).



Thank You For Your Order!

Dear Michael Walsh,

Thank you for placing your order through Copyright Clearance Center's RightsLink service. Elsevier has partnered with RightsLink to license its content. This notice is a confirmation that your order was successful.

Your order details and publisher terms and conditions are available by clicking the link below:
<http://s100.copyright.com/CustomAdmin/PLF.jsp?ref=514403a6-7c63-4c00-a09c-e8dd66ca7afa>

Order Details
Licensee: Michael T Walsh
License Date: Nov 6, 2013
License Number: 3263130030774
Publication: Corrosion Science
Title: Kelvin Probe electrode for contactless potential measurement on concrete - Properties and corrosion profiling application
Type Of Use: reuse in a thesis/dissertation
Total: 0.00 USD